PERGAMON

Progress in Aerospace Sciences 36 (2000) 629–654

PROGRESS IN AEROSPACE SCIENCES

www.elsevier.com/locate/paerosci

Data and performances of selected aircraft and rotorcraft

Antonio Filippone*

Department of Energy Engineering, Technical University of Denmark, Building 404, DK-2800 Lyngby, Denmark

Abstract

The purpose of this article is to provide a synthetic and comparative view of selected aircraft and rotorcraft (nearly 300 of them) from past and present. We report geometric characteristics of wings (wing span, areas, aspect-ratios, sweep angles, dihedral/anhedral angles, thickness ratios at root and tips, taper ratios) and rotor blades (type of rotor, diameter, number of blades, solidity, rpm, tip Mach numbers); aerodynamic data (drag coefficients at zero lift, cruise and maximum absolute glide ratio); performances (wing and disk loadings, maximum absolute Mach number, cruise Mach number, service ceiling, rate of climb, centrifugal acceleration limits, maximum take-off weight, maximum payload, thrust-to-weight ratios). There are additional data on wing types, high-lift devices, noise levels at take-off and landing. The data are presented on tables for each aircraft class. A graphic analysis offers a comparative look at all types of data. Accuracy levels are provided wherever available.

Contents

* Tel.: + 45-45-25-43-24; fax: + 45-45-93-06-93.
E-mail address: afb@et.dtu.dk (A. Filippone).

0376-0421/00/$ - see front matter
PII: S0376-0421(00)00011-7

Nomenclature

A	wing area; rotor disk area (m^2)
$\mathscr{AR}$	wing geometrical aspect-ratio
b	wing span (m)
B	main rotor's number of blades (rotorcraft)
c	wing/blade chord (m)
C_D	drag coefficient
C_L	lift coefficient
$C_{L_{max}}$	maximum lift coefficient
C_f	skin friction coefficient
d	rotor diameter (m)
d_{tail}	tail rotor diameter (m)
d'	equivalent wing span (m)
D	drag force (N)
e	wing efficiency factor
E	maximum cargo range
g^+	maximum normal acceleration, g-limit
h	hovering ceiling, out of ground effect (m)
k	reduced frequency
l	aircraft length, or length scale (m)
L	lift force (N)
LE	leading edge line
M	Mach number
n	normal load factor
P_L	max power loading = MTOW/T (kg/kN for jets; kg/kW for propellers)
P_s	specific excess power (m/s)
QC	quarter chord line
q	dynamic pressure ($kg\ ms^{-2}$)
R	aircraft range (km)
Re	Reynolds number
R_C	rate of climb (m/min)
t/c	wing thickness ratio
T	take-off thrust rating (kN), International Standard Atmosphere (ISA)
u	aircraft's speed (km/h, or m/s)
U_s	aircraft's stalling velocity with flaps down (km/h)
W/A	max wing loading = MTOW/A (kg/m^2); also equivalent disk loading
Z	service ceiling in sustained horizontal flight (m); vertical coordinate
α	angle of attack (deg)
β	dihedral angle, if >0; anhedral if <0 (deg)
λ	taper ratio = c_t/c_r
Λ	wing sweep around LE or QC, as specified (deg)
γ	angle of climb (deg)
μ	advance ratio
ρ	air density (kg/m^3)
σ	rotor solidity
$\dot{\Theta}$	maximum sustained rate of turn (deg/s)

Subscripts/superscripts

$[]_{cr}$	cruise conditions
$[]_r$	root
$[]_t$	tip
$[]_0$	at zero lift
$[]_v$	viscous

Aircraft wing specifications

BWB	blended wing body
FSW	forward swept wing
SBW	swept back wing
VSW	variable sweep (usually discrete positions)
Δ	conventional delta wing
Δ^2	double delta wing

Rotorcraft specifications

AT	attack, anti-tank, anti-submarine, advanced military vehicle
C	cargo, crane, heavy lift transport (usually military vehicle)
GE	civil/military general purpose vehicle (patrol, rescue, transport)
LC	light commercial vehicle (for a few passengers and limited freight)
UT	military utility vehicle (troops, freight, matériel, support operations)
TW	twin or tandem rotor, utility vehicle with two rotor shafts
TR	tilt rotor vehicle

Other symbols and abbreviations

AoA	angle of attack
EPNdB	effective perceived noise, measured in dB
LERX	leading-edge root extension
MTOW	maximum take-off weight (kg)
OWE	operating empty weight (kg)
PAY	payload (kg)
P/O	PAY/OWE
P/W	PAY/MTOW
rpm	rounds-per-minute (rotor speeds)
V/STOL	vertical/short take-off and landing
SSF	single-slotted TE flap
DSF	double-slotted TE flap
TSF	triple-slotted TE flap
SL	single LE slat
SLK	LE Kruger slat
USB	upper surface blowing
VT	vectored thrust

Aircraft designation

Aircraft and rotorcraft are identified by company name (Antonov, Lockheed) + designation (An-124, F-117) + version (A, B); nickname (Ruslan, Raptor) is rarely used. In the graphics the company names are added only occasionally. Refer to the data base [1] for full information and data that for clarity are not labelled.

1. Introduction

The conceptual design of an aircraft and its aerodynamic analysis may require a fair amount of independent parameters. Quantities as essential as the wing aspect-ratio have different optima, depending on whether the figure of merit is the acquisition cost, the direct operating costs, the take-off gross weight, or the block fuel [2].

Engineers have long recognized that there is no simple solution, and in recent years new multi-disciplinary methods have been devised to treat design problems in complex search spaces. Even then, first guess solutions may be required, and often operation points falling off the known space are indication of something new.

It is estimated it took C. Lindbergh and his team at Ryan Aircraft about 46 days to design and build the successful *Spirit of St. Louis* (1927), and K. Tank one year from conception to first flight of his transatlantic Focke Wulf Fw-200 (1935). To this day records are broken in the opposite sense: the B2-A required 24,000 h of wind tunnel testing, 44,000 h of avionics testing, 6000 h of control systems testing, and 4000 h of flight testing, for a grand total of approximately 78,000 h [3]. At the same time, some aircraft are known to consist of one million parts, for example Lockheed-Martin F-22: "Designing anything that complex takes more than dazzling engineering" [4].

The increasing level of technology has led to ever increasing sophistication, while the concomitant increase in analytical, computational and simulation capabilities has not kept the pace. Hence the increasing development times, that in some cases has reached the 10 year mark. There is a general feeling that this trend must be stopped and even reversed.

Although the initial phase of conceptual design is rather fluid, with several ideas tested, accepted, rejected, the use of tabulated data to compare past and current technology is an invaluable aid. Most conceptual designs can be defined as *conservative* whenever their operation points fall within the range of known performances. Consideration of reference data seldom can be discounted.

This paper responds to the need of a broad survey of existing data in conventional aircraft and rotorcraft, and provides useful information for aerospace sciences. The presentation will stick to data and performances related to aerodynamics and propulsion systems of full-scale vehicles. Structures, costs and commercial issues are not discussed. Out of the discussion are also all those parameters that are difficult to define with any certainty, or are not readily available in the unclassified literature, or cannot be presented concisely. Data in this class include all the unsteady aerodynamics characteristics, the aerodynamic derivatives, passenger details and most ranges and fuel capacity. Seckel [5] in his book on dynamics and stability reports a few interesting examples of these characteristics.

The vehicles included in the analysis are organized according to class. This selection provides maximum order and well consistent trends. In some cases comparisons are performed across the whole spectrum of aircraft and rotorcraft. There are several ways of reading the data. One is the historical trend. This requires a selection of design cases to be plotted against a time line (*technology trends*). Another option is to compare many vehicles in the same class, to discover trends dictated by old or new design considerations, and experimental work (*iso-technology*). The curves fit are either lines or power curves. The best fit is no minor issue, but efforts have been done to select the curves that best represent the raw data.

Some aircraft classes are defined in a very narrow design space (for example twin turboprops for regional transport), while others (V/STOL vehicles, both military and civil utility) show scattered operation points, also due to the more complex propulsion systems. The latter vehicles are not considered in this study. A partial review is available in [6,7]. Some interesting data on all types of Soviet/Russian aircraft have been published by Gurton [8]. A systematic, analysis of aircraft size prior to 1970 was published by Cleveland [9]. Other useful data have been published by Poisson-Quinton [10] and Loftkin [11]. From a general point of view, there is plenty of literature on why airplanes look the way they do. Among the most remarkable ones, there is Küchemann's classical textbook [12], and Stinton's airplane anatomy [13].

The data and performances presented in this study have been collected, elaborated, averaged and approximated from a number of sources, consisting of partial data bases, flight and wind tunnel data, technical drawings. The references are limited to the sources of extensive information used for the compilation of the data base.

The data that have been directly elaborated include: rotor solidity, tip Mach numbers, advance ratios, rotor disk loadings (rotorcraft); wing aspect-ratios, taper ratios, thrust-to-weight ratios and some sweep angles (around quarter-chord and leading-edge), some dihedral angles and many lift and drag coefficients (aircraft).

The material is arranged as follows: we first discuss the aerodynamic data, then selected performance parameters, and finally some essential geometric characteristics, for all the vehicles. In the last section we analyze vehicles in each class for selected classes only.

All the geometrical quantities have been considered as in the aerospace practice (described for example by the AIAA [14]), with a few additional specifications, as reported in Section 5.

Data and performances labelled as *best* are restricted to the records available in the unclassified literature; they are in no way absolute values. SI units are used throughout (with the exception of wing loading and rotor disk loading, for which we used the engineering units kg/m^2).

The choice of the vehicles deserves a note of discussion. While we have attempted to analyze the data, we have collected information relative to about 300 vehicles, mostly from the present time, and some from as far back as the Second World War. Many aircraft had to be excluded, because their operation points looked similar to each other (for example, business jet aircraft and regional transports) or because their data were incomplete. Some aircraft classes, such as light aircraft have been left out of the discussion on purpose, because we wanted to concentrate on vehicles performances that we assumed to be outstanding.

2. Reliability of the data

All the aircraft are very likely to evolve slowly over the years. Brand new designs, instead, are less and less likely to land on the design board. Fig. 1 shows a historical graphic with the number of wind tunnel hours before maiden flight for selected aircraft. The Wright Flyer is believed to have required about 20 h, while the US Shuttle over 25,000 h (all aerodynamic parts, and all speeds of interest) in multiple test facilities.

Sometimes a major re-engineering project takes place (like new powerplant installations, engine integration, surface cleanup). Besides, virtually all types of aircraft and rotorcraft are built according to customers' specifications, or under license, which can introduce further differentiations. Therefore, it comes to mind to say that *no two aircraft are ever the same*, though no one emphasizes this fact. For military vehicles there is often the risk of handling *unconfirmed data*.

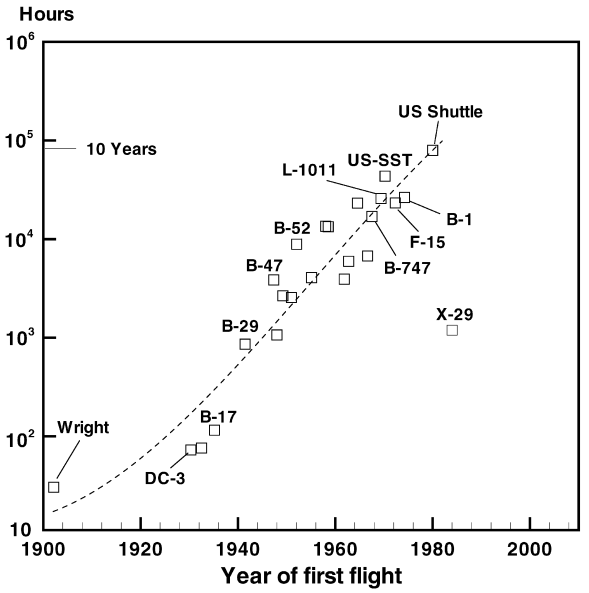

Fig. 1. Demonstrated wind tunnel times before first take off.

For any given aircraft the data are still difficult to read. Take for example the $C_{L_{max}}$: this can be for the 2D airfoil, for the 3D wing, for the aircraft model in wind tunnel, for the aircraft in flight testing, at take-off or landing, with control surfaces fully extended, or even the certified performance, which is different from all the above. Most of the technical literature is not clear about the test conditions (an exception is provided by Hopps and Danforth [15]). Items are left blank wherever details could not be obtained.

The data are sometimes well correlated, other times rather lie in a broadband, for a number of reasons: (1) data may be fudged by manufacturer or operator of the aircraft; (2) data refer to operating conditions not clearly specified; (3) data indicate non-conventional designs; (4) data are from old aircraft designs; (5) data and performances have been erroneously interpreted.

All the data provided are subject to change, some more rapidly than others (except, of course, for the aircraft that are now out of production). Rapid changes can occur on engine installations and fuselage dimensions; slow changes usually occur on wing configurations. The wing system remains the core of the aircraft, even at times of fully integrated avionics and satellite flight control. A new wing generally brings a new airplane.

3. Aerodynamic data

The values of the lift and drag coefficients depend on the operating angle of attack, α, and cruise Mach

number, M. Reporting complete data would require polars for all the aircraft considered. Most of these data are not public, although some useful information is available for selected aircraft [16–20].

Some data produced in the technical literature refer to scale wind tunnel models, half-models, mock-up models, research models; these are not interesting for our investigation. The correlation between wind tunnel models of any scale and flight data is not always straightforward. One of the reasons is attributed to the scale effects. It has been noted that scaling has consequences on the largest aircraft, whose boundary layers are fully turbulent. The wind tunnel Reynolds numbers, in fact, are often lower than the full-scale flight Reynolds numbers, that creates boundary layers that are partially laminar.

An example of aircraft polar is shown in Fig. 2 where these operation points have been denoted: (1) the drag coefficient at zero lift, C_{D_0}, that gives an idea of the combined viscous, wave and interference drag; (2) the glide ratio at cruise conditions $(L/D)_c$; (3) the absolute maximum glide ratio $(L/D)_{max}$; (4) the $C_{L_{max}}$ at 1-g (i.e. steady-state conditions).

These polars can be derived for any flap and slat setting, but landing and take-off configurations are the most important ones. Other graphics of interest include the $C_L - \alpha$ map, that highlights the effects of the control surfaces on the $C_{L_{max}}$.

3.1. Drag coefficients

The technical literature on aircraft drag is vast, and is obviously concerned with all the aspects of drag analysis and reduction, besides issues related to aircraft design. At any rate, drag data are particularly difficult to gather: the common practice is to not to show the tick labels on the axes of drag polars, or to provide drag savings in percent against a baseline that is not known.

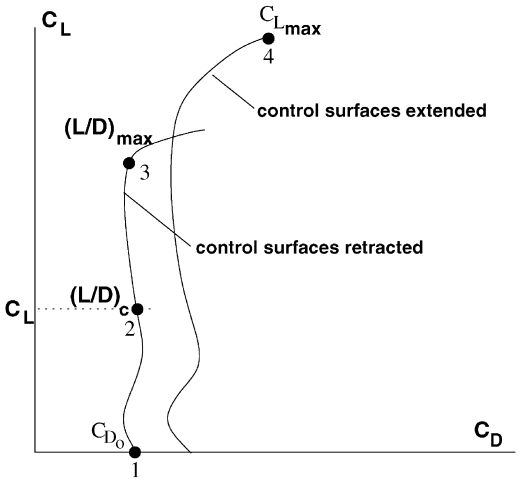

Fig. 2. Generic aircraft polar, with the relevant operation points. Two settings shown.

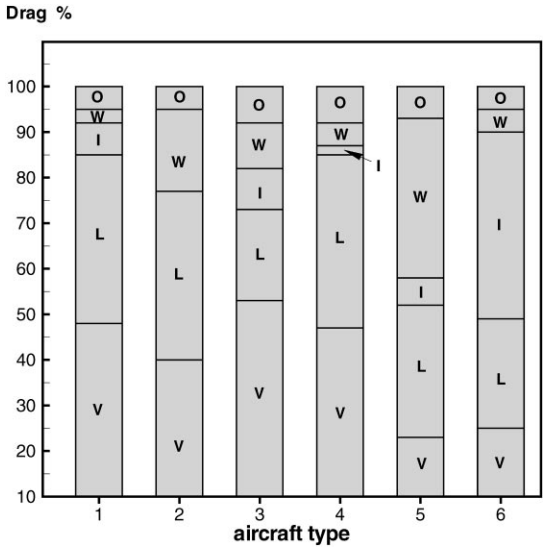

Fig. 3. Drag build-up on some aircraft types: 1 = subsonic transport aircraft; 2 = supersonic transport; 3 = executive jet; 4 = fighter at subsonic speed; 5 = fighter at supersonic speed; 6 = civil utility helicopter. Drag causes: L = lift-induced; V = viscous; I = interference; W = wave; O = other.

The typical drag build-up on some aeronautical systems is shown in Fig. 3 (elaborated from [21,22]). The drag components are averaged from a number of data, and may shift a few percent on either direction, depending on aircraft and cruise conditions. This analysis serves to show in which direction technological advances may produce effective drag savings and fuel economy. There is quite an amount of information that can be extracted from Fig. 3. For example, the wave drag is a minor problem in today's airliners, while the lift-induced drag and the viscous drag make up most of the total count. Civil utility helicopters are instead characterized by large interference effects, first and foremost the rotor-fuselage interaction, which accounts for an estimated 40% of the total drag.

The analysis shows that the zero-lift drag coefficient, C_{D_0}, for propeller-driven aircraft (light airplanes and business turboprops) is in the range of 0.02–0.04. For subsonic jet transports the figures are lower: $C_{D_0} \sim 0.013$–0.020, with average skin friction coefficients $\bar{C}_f \sim 0.0025$–0.0060 (all aircraft types). The lowest $\bar{C}_f$ values are found on commercial jets, that have smooth surfaces. Gaps around windows and doors, panel joints, mis-rigged controls, antennas, etc., contribute to C_{D_0} in a measure of several drag counts, or up to 3–4% of the total drag.

The surface *clean-up* occurred over the years is shown in Fig. 4, that shows skin friction drag levels for selected

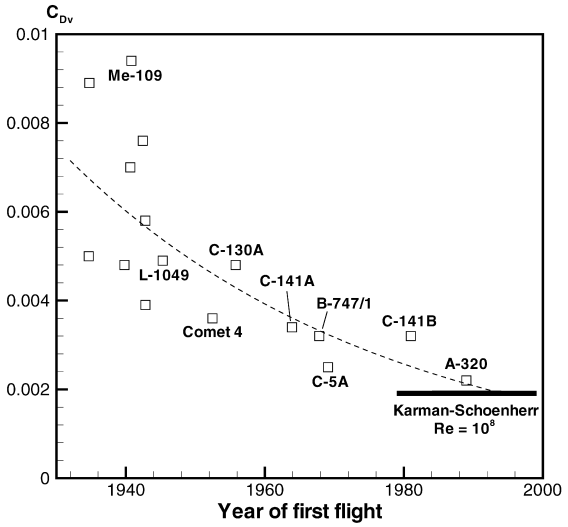

Fig. 4. Estimated viscous drag coefficient C_{D_v} at year of first flight.

aircraft at year of first flight. For the Airbus A-320 we have estimated the viscous C_{D_v} with surface riblets over 75% of its wetted surface [23]. The technological progress is impressive, although most of the drag reduction methods devised (boundary layer control, suction and blowing; large-eddy break-up devices, and not least riblets) remain within the research domain. Current technology is reaching a plateau roughly corresponding to the fully turbulent boundary layers. The data are compared with the average turbulent C_D for a flat plate (von Kármán–Schönherr) at $\mathrm{Re} = 10^8$.

The lift-induced drag is defined by

$$C_{D_i} = \frac{C_L^2}{e\pi\mathscr{A}\mathscr{R}}. \tag{1}$$

The efficiency factor e (with respect to ideal elliptic loading) is of the order 0.74–0.80 for many subsonic jet airplanes [24]), lower for other airplanes.

Experience from the past shows that it is indeed possible to reduce the cruise C_D of an aircraft by several drag counts, which translates into some relevant percent values. For example, re-engineering of the cargo C-141 Star Lifter in the early 1980s achieved a remarkable 8% drag saving [25]). Equipping the Boeing B-747-400 with winglets yields a 3% fuel saving over long-range cruise; applications of surface riblets on the Airbus A340-300 in 1997 intended to reduce fuel consumption by 3–4 metric tons/year (Jane's Information Systems, 1998 [3]). Rear fuselage re-design can save 1% drag (ATR-42, Concorde). However, nearly every successful aircraft is a design case.

Table 1 summarizes the aerodynamic data of some important design cases. Case 1 shows the effects of aerodynamic design from a base wing (the Gulfstream II business jet), using advanced supercritical wing sections, reduced wing sweep and winglets. The result was a 14% drag saving at constant lift coefficient. Case 2 shows the effects of aerodynamic improvements on a military cargo aircraft (Lockheed C-141): Afterbody, wing-body and landing gear hold added to an 8% drag saving, other operating parameters being the same. Case 3 is the effect of transonic drag rise on a research fighter aircraft, the YF-16. Case 4, the North American XB-70A, was a high-speed research program, and its data are compared at three different operation points.

Drag levels for the helicopter are much higher, because of the bluff body design, fuselage–rotor interaction, free standing landing gear, external stores, and surface roughness. A good drag coefficient in forward flight is $C_D \sim 1$ (Aerospatiale AS 365N). This is about 50 times higher than an average commercial jet aircraft. The scaling of the drag forces is done with the wing area for aircraft and rotor disk area for rotorcraft, therefore the comparison between drag coefficients is not fully appropriate. A more fair comparison can be done with the ratio D/q, where $q = \rho u^2/2$ is the dynamic pressure.

Table 1
Drag and lift data of some aircraft

	Aircraft	C_D	C_L	M	$M\,L/D$	$\mathscr{A}\mathscr{R}$	Z	Notes
1	Gulfstream II	0.0305	0.45	0.72	10.62	7.3		Plain wing
	Gulfstream III	0.0262	0.45	0.74	12.71	7.4		W/winglets
2	Lockheed C-141A	0.0246	0.40	0.77	12.52	7.9		
	Lockheed C-141B	0.0228	0.40	0.77	13.51	7.9		Redesigned
3	General Dynamics YF-16	0.026	0.40	0.90	13.85	3.2	9840	Transonic
		0.083	0.40	1.60	7.71	3.2	9840	Supersonic
4	North American XB-70A	0.0106	0.080	0.76	5.74	1.75	5085	Transonic
		0.0223	0.115	1.21	6.22	1.75	10,630	Supersonic
		0.0158	0.161	2.39	24.35	1.75	18,405	Supersonic

3.2. Lift–drag ratio

The glide ratio L/D (also called *finesse* or *glide number*) is reached at $C_L \sim 0.4$–0.5 in subsonic flight; much lower lift values are required at supersonic speed: $C_L \sim 0.10$–0.15. For commercial subsonic jet aircraft $(L/D)_{max} \sim 17$–20, that is in the same range of the best L/D achieved by some birds, for example the California Condor and the Great Albatross [26]. The highest $(L/D)_c$ on record is that of the Boeing B-52G, $L/D \sim 20.5$.

While improvements are still possible with non conventional designs [27], the data indicate that technology has already achieved performances fully comparable with those of the natural flight.

Some aircraft L/D are shown in Fig. 5 as function of the cruise Mach number. There is a large spread in the data at all Mach numbers. The XB-70A, lowest point at $M < 1$ (see also Table 1), was designed for high supersonic speed ($M = 3$), and shows poor performances a low supersonic speeds. The relatively good L/D of this aircraft is attributed to the *compression lift* generated at the highest speeds [28]. Other low values are obtained with supersonic fighter jets. The operational range is noted by a shaded box. The expression

$$\left(\frac{L}{D}\right)_c = 4\left(1 + \frac{3}{M}\right) \tag{2}$$

is generally assumed as a benchmark to define a band of state-of-the-art values at supersonic speeds [12]. Eq. (2) yields $L/D = 19$ at $M = 0.8$, and $L/D = 10$ at $M = 2$. At supersonic speeds the aerodynamic performances deteriorate sharply, due to the effects of the shock waves.

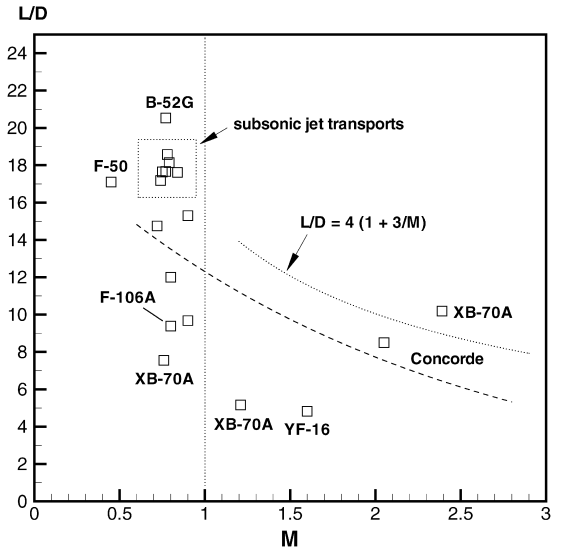

Fig. 5. L/D as a function of the cruise Mach number (all aircraft). Dotted line is a power fit.

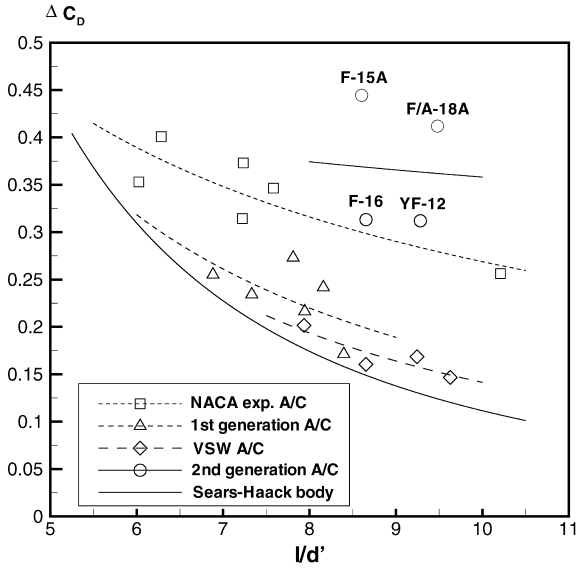

Fig. 6. Transonic drag rise for some supersonic fighter aircraft.

The transonic drag jump is usually compared by taking values at $M = 0.8$ and 1.2. This difference can be of the order $\Delta C_D \sim 0.4$–0.5, as shown in Fig. 6 (data gathered from Poisson-Quinton and Boppe). The figure shows data in four bands, each consisting of an aircraft class.

The ratio l/d' in the abscissa is the *equivalent slenderness* of the aircraft, with $d' = (4S_{max}/\pi)^{1/2}$, and S_{max} the aircraft's maximum cross-sectional area. The drag jump decreases with the increasing slenderness, and is strongly dependent on the amount and types of external stores. Minimum penalties are of course obtained with clean configurations. For reference, also the drag of the Sears–Haack body having the same slenderness l/d' is shown. This is a body of minimum wave drag at supersonic speed, whose theoretical value is independent of the speed [29]

$$C_{D_w} = \frac{9}{8}\pi^2 \frac{1}{(l/d')^2}. \tag{3}$$

The Sears–Haack body does not exhibit a drag jump through the speed of sound (Eq. (3)). For a slender aircraft the wave drag would be negligible at high subsonic speeds, therefore the Sears–Haack body would be a better reference data.

Since the aircraft cruise range is proportional to the *range factor* $M(L/D)$ (Breguet), a relative drop in efficiency may be offset by a correspondent increase in Mach number. This term is useful to compare performances at subsonic and supersonic speeds. From our data we find for the B-52G $M(L/D) \sim 16$, for the Concorde ~ 17, and

for the XB-70A ~ 24. The benchmark values are found from Eq. (2) multiplied by M.

3.3. Cruise lift and high-lift performances

Landing and take-off speeds depend on the maximum lift that can be produced by the aircraft through its control surfaces. These can be unpowered multi-element wing systems (most cases) and powered systems: over-the-wing blowing (YC-14, An-72/74), vectored thrust (Lockheed C-17A, Lockheed F-22A, Sukhoi S-37), propulsive (*direct*) lift (BAe Sea Harrier, Harrier II).

$C_{L_{max}}$ figures for unpowered high-lift systems are in the range 2.0–3.0; with powered systems $C_{L_{max}} \sim 8$–10 have been reported, although not all systems successfully tested on experimental aircraft have been applied [7,30,31].

Table 2 summarizes the high lift systems for some aircraft (see nomenclature for symbols). These aircraft have complex mechanical systems that consist of several spanwise segments.

Leading-edge elements are either rigid slats or Kruger flaps, with a variable camber, and therefore are more flexible. Trailing-edge devices consist of up to three elements. In some fighter aircraft there is a leading-edge droop (BAe Hawk 200). The function of the multi-element wings is to increase the effective wing area, the effective camber, the pressure suction peak, and to provide boundary layer control. Ref. [32] discusses both aircraft design problems and state-of-the-art computational methods for high lift.

Case 1 refers to two different versions of the same commercial jet aircraft, the DC-9. In a later version, the model -30, the Douglas corporation added a LE slat, with a new LE design of the main wing to accommodate the retracted slat and an extended wing chord. Vane and flap geometries are the same.

Case 2 is a twin turboprop for short-range transport. The estimated $C_{L_{max}}$ at cruise, take-off and landing configurations is shown, with the corresponding setting of the flap angle.

Case 3 is a selection of wide body long-range subsonic jets with TE flap systems of increasing complexity. In particular, the B-747 features a variable camber Kruger slat at the LE.

Case 4 is given by two heavy lift military transports of the Lockheed company.

Case 5 is an example of powered lift systems (upper surface blown flap and vectored thrust), with estimated average performances at landing. The YC-14 also features a boundary layer control system at the wing's leading edge.

Case 6 is a comparison between two supersonic military jets, the experimental X-29A, with forward swept wing, and the SAAB JA 37, with close-coupled foreplane-Δ wing (called double Δ). In both cases high lift is obtained by controlling the downstream vortex flow on the main wing through the canards/foreplanes, the latter ones equipped with their own control surfaces.

Fig. 7 shows the technological progress toward improved high-lift systems. The aircraft are ordered by increasing complexity of their control systems. The only two examples of powered systems in the graphic have minimum limits above the best performances obtained with triple-slotted Fowler flaps (TSF) and Kruger slats.

Table 2
High-lift systems and estimated $C_{L_{max}}$ for some aircraft

Case	Aircraft	LE	TE	$C_{L_{max}}$	Notes
1	Douglas DC-9-10	—	DSF	2.50	1-g flight data
	Douglas DC-9-30	SL	DSF	2.73	1-g flight data
2	ATR-42	—	DSF	1.75	1-g flight, $\delta_f = 0^\circ$ (cruise)
				2.61	1-g flight, $\delta_f = 15^\circ$ (take-off)
				3.15	1-g flight, $\delta_f = 27^\circ$ (landing)
3	Airbus A-340-300	SL	SSF	2.54	
	Lockheed L-1011	SL	DSF	2.48	1-g flight data
	Boeing B-747-100	SL Kruger	TSF	2.43	2D multi-element
4	Lockheed C-5A	SL	SSF	2.27	
	Lockheed C-141B	SL	DSF	2.25	
5	Boeing YC-14	SL Kruger	TSF + USB	3.57	Avg. flight data, landing
	MD C-17A	SL	DSF + VT		
6	Grumman X-29A	coupled canard/FSW wing		1.34	1-g flight, $M = 0.9$
	SAAB JS 37	coupled forewing/Δ wing		n.a.	

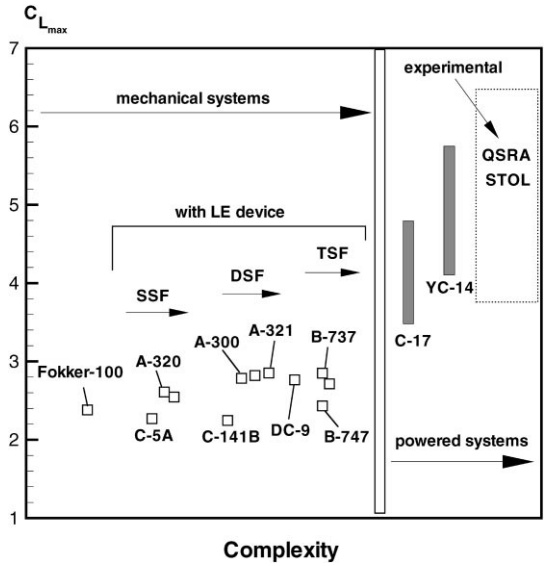

Fig. 7. $C_{L_{max}}$ versus complexity of the high lift system for selected production aircraft (except YC-14). The graphic also shows the boundary between mechanical systems (unpowered) and powered systems.

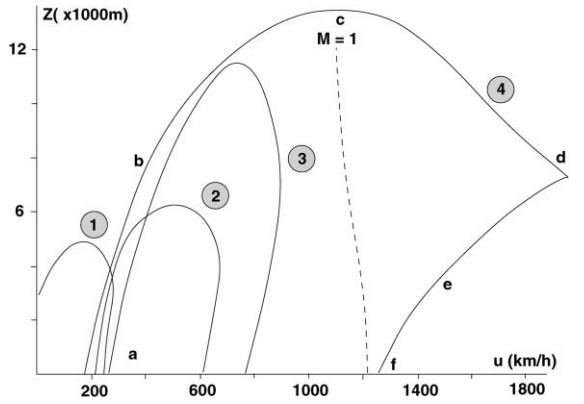

Fig. 8. Typical aircraft flight envelopes: 1 = MD AH-64D (helicopter); 2 = Lockheed C-130J (cargo); 3 = Airbus A-300 (subsonic transport) ; 4 = Lockheed F-16/C (supersonic fighter).

4. Selected performance data

As for the aerodynamic characteristics, full data for the aircraft performances would require knowledge of all the aircraft flight envelopes. Here again we choose particular operation points: maximum absolute speed in horizontal flight, cruise Mach number at altitude, stalling velocity with control surfaces at full extension (some aircraft types), service ceiling, hover ceiling out of ground effect (rotorcraft only). Other specific performance parameters are discussed in the section concerning the comparative analysis.

An example of flight envelopes is shown in Fig. 8, where the critical operation points are noted for 4 types of aircraft (these envelopes have been extrapolated from the available data).

Envelope 4 is for clean configuration and afterburning thrust. For this aircraft, as well as other aircraft in the same class, flight envelopes are dependent of the external stores. The actual maximum speed at maximum thrust at given altitude is dependent on drag and aircraft gross weight.

4.1. Mach number

The values provided depend on the type of aircraft. For commercial aircraft (subsonic jets, twin turboprops, business jets) M is the economic long-range cruise Mach number (± 0.02). At the operating lift coefficient M is close to the point where the transonic drag starts to build up (this point is about 90–93% of the maximum absolute speed with supercritical wing section).

For fighter aircraft the Mach number reported is the absolute maximum in the aircraft flight envelope.[1] This speed can be sustained for a short time over a narrow range of altitudes (*supersonic dash*), as shown in Fig. 8 (envelope 4). Most of the aircraft in this class can fly for a long range only at transonic speeds; a few are able of maintaining supersonic Mach numbers at all altitudes, including sea level (*supercruise*).

The reason for this apparent discrepancy in the database is that the absolute Mach number for commercial jets is of lesser interest, because the aircraft is never operated at that speed.

4.2. Normal acceleration limits

The g^+-limits are the absolute maximum centrifugal accelerations an aircraft can sustain during transonic or supersonic maneuver before incurring structural damage. This limit is dependent on the type and number of external stores, mission set up and speed. The maximum accelerations are obtained at transonic speeds. The negative acceleration limits, g^-, are much smaller. For fighter and attack aircraft $g^- \sim g^+/2$; for rotorcraft (mostly AT-vehicles) it is reasonable to assume $g^- \sim g^+/3$. For supersonic fighters the best values are $g^+ = 8$–9 at transonic speeds, $g^+ = 6$–7 at supersonic speeds. The best rotorcraft g^+-limits are $g^+ = 3$. Acrobatic airplanes perform even better, with $g^+ \sim 12$ or higher (see Table 6).

[1] The data provided are reached with afterburning thrust and a clean configuration.

4.3. Rate of climb

The absolute maximum rates of climb, R_C, are provided, except for all the turboprops, whose data are for sea level conditions. The highest R_C are reached at altitudes that depend on the aircraft, namely of the engine thrust rates and the aerodynamic efficiency. In steady flight the rate of climb assumes a simple expression

$$R_C = u\left(\frac{T}{W\cos\gamma} - \frac{D}{L}\right), \tag{4}$$

where γ is the angle of climb. If the angle of climb is small (typically less than 10°), then

$$R_C \simeq u\left(\frac{T}{W} - \frac{D}{L}\right) \tag{5}$$

is a good approximation. The R_C in Eqs. (4) and (5) is given in m/s, but the technical practice is to express this data in m/min. Fighter jets reach $R_C \sim 10{,}000$–$18{,}000$ m/min, with the MiG-29 claiming $R_C \sim 20{,}000$ m/min. This corresponds to a vertical climb of about 20 body lengths per second!

For rotorcraft the values reported are obtained in inclined forward flight. Climb rates in vertical flight are lower. Typical values are $R_C \sim 500$–800 m/min for state-of-the-art AT-vehicles, lower for all other types. The AT helicopter Kamov Ka-29 claims $R_C \sim 890$ m/min, which corresponds to about 0.9 rotor diameter lengths per second. If we consider average data, $R_C \sim 0.6$–0.7 diameter lengths per second.

4.4. Hover ceiling

The hover ceiling of a helicopter is the altitude at which the rate of climb is zero. This is evaluated out of ground effect (OGE) and in ground effect (IGE), at standard atmosphere (ISA) or otherwise. Some OGE-ISA (free flight) data are reported in Table 4.

IGE hover data are needed to assess at which altitude and atmospheric conditions the helicopter is able to take-off. Since the rate of climb is $R_C = \mathrm{d}Z/\mathrm{d}t$, the hover ceiling is reached when the air density (depending on altitude and temperature) is no longer enough to extract power from the engine. The data from flight tests are very scattered, with limits from 800 to 8000 m.

4.5. Maximum take-off weight and other weights

MTOW includes the aircraft's operating empty weight (OWE), the payload (PAY) and the fuel. Sometimes the symbol W is used for weight, which is not necessarily equal to MTOW. For military aircraft and rotorcraft it is subject to speculation, because the MTOW depends on the war-load, on the mission requirements, the operating environments, and even on customers specifications. For example, the aircraft Grumman A-6E is reported to have a MTOW $\sim 27{,}400$ kg for take-off from field, and MTOW $= 26{,}800$ kg, if take-off is assisted by catapult on aircraft carrier. This MTOW is also susceptible to increase in later versions of the same aircraft.

For heavy lift helicopters values of MTOW are given for internal loads (i.e. inside the aircraft). Some vehicles are able to operate with oversize slung loads (Mil-10 and Boeing-Vertol CH-47D). We report only the performances for maximum internal payload. The remaining data are conforming with this convention.

4.6. Wing loading

The maximum wing loadings W/A are computed using the MTOW and the wing area as defined above. For VSW aircraft the area at maximum sweep has been used, when available. Wing loading is not computed for BWB-aircraft. Fig. 9 shows the W/A trends versus the aircraft Mach number. If the supersonic aircraft are shifted to transonic flight condition ($M = 0.8$–0.85) the data are clean, with wing loadings well correlated by an exponential fit.

4.7. Noise levels

Noise emissions are expressed in effective perceived noise, in dB (EPNdB), as certified by the international authorities[2] for each aircraft type and for specified conditions: take-off, fly-over/landing, and sideline, at standard

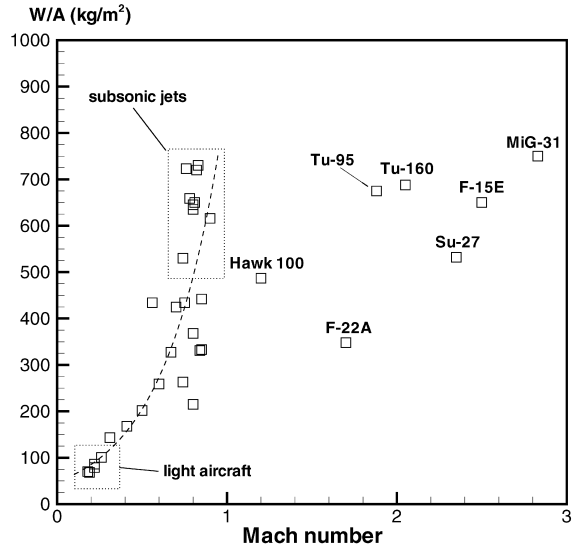

Fig. 9. Aircraft wing loading trends (selected aircraft).

[2] ICAO, Chapter 3, Annex 16; Far, Part 36, Stage 3.

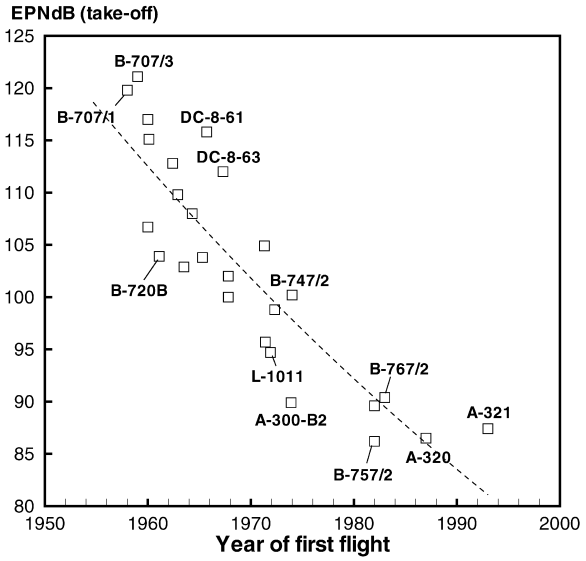

Fig. 10. Noise levels at take-off for commercial jets.

points in the neighborhood of the runway. These are as follows:

- EPNdB at take-off: measured at 6500 m from brake release along the runway centerline.
- EPNdB at landing/approach: measured 2000 m from landing point on runway.
- EPNdB at sideline; measured 450 m (2–3 engines aircraft) or 570 m (4 engines) from runway centerline.

The noise levels reported are those certified for standard engines. They are subject to change, as new high by-pass engines are developed and regulations become tighter. Fig. 10 shows a technology trend in noise emissions and corresponding limits. An average reduction of over 25 dB has been achieved over the past 30 years. The first generation of Boeing 707 created a noise at take-off similar to that of the Concorde. As noted by Crighton [33], this was as much noise as produced by the world population shouting together. A Boeing 737 of 30 years later produced as much noise as the city of New York shouting in phase.

Fig. 11 is an iso-technology summary comparing all classes of aircraft and rotorcraft in the year 2000. In the data recorded, the highest noise levels are those of the Concorde (over 120 dB at take-off). The least noisy aircraft are in the category of the business jets (72–82 EPNdB). Data for some light and utility helicopters are also shown. Extensive data are reported by Lowson [34], and Cox [35].

Sonic boom effects are another class of noise-related issues. Boom overpressure on the ground is estimated at $\Delta p \sim 0.51$–$0.78\,\mathrm{kg/m^2}$ (5.0–7.6 Pa). Data for Lockheed SR-71A at $M = 1.26$ are $\Delta p \sim 0.614\,\mathrm{kg/m^2}$ (6 Pa) at all flight altitudes.

5. Geometrical data

5.1. Wing geometry

The wing geometries come in a bewildering amount of shapes and sizes. They include straight wings with a small sweep angle (most single-engine light aircraft); conventional swept back (for low and high subsonic flight); forward swept wing (for extreme agility and high angle of

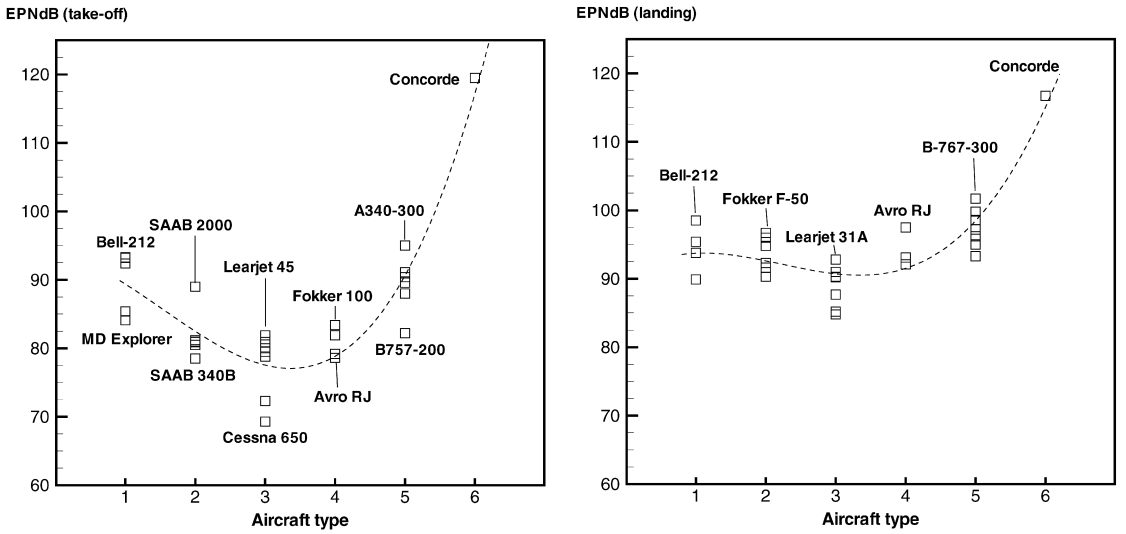

Fig. 11. Noise levels at take-off and landing in EPNdB as certified for different classes of aircraft: 1 = helicopters; 2 = twin turboprops for regional transport; 3 = business jets; 4 = regional jets; 5 = subsonic commercial transports; 6 = Concorde.

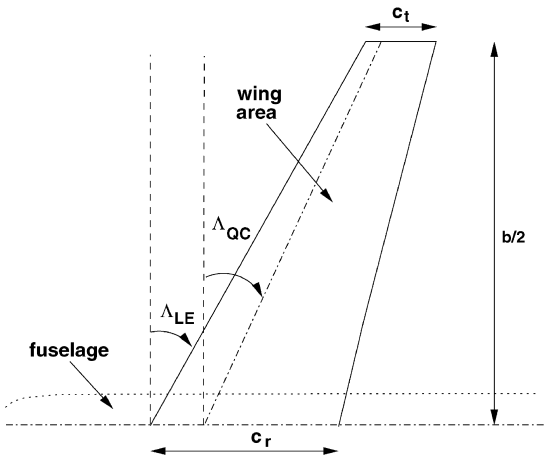

Fig. 12. Typical wing geometry, with essential characteristics.

attack operation at both transonic and supersonic speeds); conventional delta wing (for supersonic flight); wings with a variable sweep (only military vehicles, fighters and bombers); blended wing bodies (or flying wings). Most of these features are listed in Table 6. The main parameters are shown in the sketch of Fig. 12.

Some fighter wings are more complicated, because they are designed to operate with leading-edge root extensions (LERX), adjustable canards (Dassault Rafale, SAAB JS39), foreplane wings. In particular, SAAB JA 35 and JA 37 feature a double delta wing, with a smaller foreplane.

The wing area is defined as the *clean* wing area projected on the ground plane, without including fillets, control surfaces, winglets, foreplanes, canards, and LERX. For the estimation of the maximum wing loading only this area is considered. The ratio of foreplane wing to main wing area generally does not exceed 10% (for example, Eurofighter 2000, Rockwell-DASA X-31), although it can be as much as 20% in some V/STOL experimental aircraft.

5.2. Wing span

The wing span, b, is the distance tip-to-tip, measured on the horizontal line with aircraft on the ground. This quantity excludes tip devices (canted winglets, tanks, sails) and tip weapons (missiles or other), and is variable in all VSW aircraft.

There is a tricky problem in the case of very large aircraft, like the Boeing B-747-400. An aircraft on the ground with maximum fuel has a wing span 0.48 m larger than that of an empty aircraft. This happens because with the deflection of the wing created by the additional weight, the winglets (canted outward by 22°) tend to open up, thus increasing the apparent wing span by 0.74%.

5.3. Aspect-ratios and shape parameters

There are two different definitions: the *geometrical* and the *structural* aspect-ratio. The geometrical aspect-ratio is $\mathscr{AR} = b^2/A$; it includes the portion of the span crossing through the fuselage. This is the definition used in the present study, and may be different from data reported elsewhere. The structural aspect-ratio is computed from the actual wing attachment to the tip, along specified lines (e.g. quarter-chord). This is a more precise measure of slenderness, and is the relevant quantity for most aeroelastic calculations.

For wings with variable sweep (VSW), $\mathscr{AR}$ more than doubles by positioning the wing at minimum sweep (for example: Sukhoi Su-24 has $\mathscr{AR} = 2.1$–5.6). Typical $\mathscr{AR}$ are as follows: $\mathscr{AR} \sim 2$–4 for fighter aircraft; $\mathscr{AR} \sim 7$–12 for commercial airplanes. Another parameter of interest is the wetted aspect-ratio

$$f = \frac{b^2}{A_{\text{wet}}} = \mathscr{AR}\frac{A}{A_{\text{wet}}}, \tag{6}$$

with A_{wet} the aircraft wetted area. The interest in this parameter is at least twofold: (1) it provides an indication of the aircraft shape, i.e. the relative size of its wings; (2) its square root is proportional to $(L/D)_{\max}$. Data for aircraft in the Airbus family are $b^2/A_{\text{wet}} = 1.3$–1.5; $f \sim 0.6$ for the Concorde, $f \sim 2.75$ for Northrop B-2 (flying wing), $f \sim 0.17$ for Lockheed SR-71A (supersonic aircraft). $(L/D)_{\max}$ data versus f have been plotted by Raymer [36].

The slenderness l/b is also important in determining the aircraft shape. Some values are listed in Table 3 according to increasing speed.

The slenderness is expected to increase with the Mach number to meet the drag constraints. The Concorde is the most slender of the aircraft in the table. Recent studies on supersonic transport (SST) indicate similar values of l/b to cruise at $M = 2.4$.

5.4. Wing sweep

Wing sweep are available either at the quarter-chord line, or at the leading-edge line. The latter definition applies well to cases such as blended wing bodies, when the leading-edge is a straight line (Northrop B-2A, Lockheed F-117A). Four quantities are needed to describe completely the wing: c_r, b, λ and the sweep angle at LE or QC, from the formula

$$\tan \Lambda_{\text{QC}} = \tan \Lambda_{\text{LE}} - \frac{1}{8b} c_r (1 - \lambda). \tag{7}$$

If some data are missing, then the sweep angle can be retrieved from technical drawings. Other formulas, using the aspect-ratio, are available [14]. The approximation to the data reported is believed to be $\pm 1°$. For special cases there is a *compound* sweep angle, arising from the

Table 3
aircraft slenderness and corresponding speed

Aircraft	l/b	M	Notes
Piper Pa-28	0.68	0.18	Straight wing
Lockheed U2-R	0.61	0.65	Long endurance
Boeing B-747-400	1.09	0.83	Subsonic jet
Northrop B-2	2.49	0.76	Flying wing
Lockheed F-117A	1.52		Low observable
Lockheed F-22A	1.40	1.70	Supersonic fighter
Tupolev Tu-160	1.52	1.88	VSW vehicle
Concorde	2.40	2.05	Supersonic transport
North Am. XB-70A	1.87	3.0	Experimental
Lockheed SR-71A	1.93	3.31	Supersonic recoinnassance
North Am. X-15A	2.27	6.3	Rocket powered
Shuttle Spacecraft	1.57		Hypersonic
NASA X-34 (est.)	2.21		Hypersonic

use of cranked wings (some Dassault business jets, Fokker F-28, Canadair RJ CL-600, Tupolev Tu-144). Sweep angles can be defined also for LERX, canards, foreplane and tailplane wings. Forward swept wings are available only on research aircraft (Grumman X-29A, Sukhoi S-37).

For VSW-aircraft A, b, $\mathscr{AR}$, and W/A are provided at maximum sweep angle. Sweep angles are generally possible at 3 or 4 discrete positions (for example: MiG-23, MiG-27, Sukhoi Su-24, Tornado ADV; Tupolev Tu-22 and Tu-160). Wing sweep in continuously variable on the GE F-111 and the Rockwell B1-B.

5.5. Airfoil sections

Many airfoil sections of low-speed aircraft (single and twin turboprops, short-range transports) from past and present have conventional geometry, namely standard NACA profiles or other profiles from open literature, with or without modifications. The most popular wing sections are the series NACA 230xx (Cessna Citation 550, many Beechcraft airplanes, helicopters Agusta A-109, PZL Sokol, Mil-6), NACA 64_4-xxx (Fokker F-27 and F-50), NACA 64_A-xxx (Lockheed C-130, F-16C; MD F-5E), symmetric NACA 00xx (Lockheed Model 185, rotor blades on Enstrom F-28), along with some Wortmann geometries, for both aircraft wings (especially gliders) and rotorcraft blades (Bell 209 and 222). In a few cases of military application, the airfoil sections are double wedges (Lockheed F-117A) and biconvex (Ching Kuo). All the vehicles flying at transonic speeds now have supercritical wing sections, while high performance helicopters (XV-15, V-22) feature advanced technology for reduced noise [37] or leading-edge droop (Agusta A-109C, Eurocopter BO-105). In recent years the improved CFD capabilities have helped design ad-hoc wing sections and three-dimensional wings (Fokker 100, Boeing B-747, B-777). This trend is likely to be followed in the future.

Wing thickness ratios (particularly at root) are dependent of the speed range of the aircraft. Fig. 13 is a plot of $(t/c)_c$ versus the cruise or maximum Mach number for all classes of aircraft. Thickness ratios at root range from 21% of twin turboprops (commuters and short-range transport), to 4% (supersonic fighters); $(t/c)_t$ can be as low as 3%. Thickness ratios are variable on all VSW aircraft. Data for the Tornado ADV are $(t/c)_r$ variable from 12 to 6%, from minimum-to-maximum sweep. Helicopter rotor blades have $t/c = 7$–15%. Blade thickness is constant on most LC vehicles and variable on all high performance vehicles.

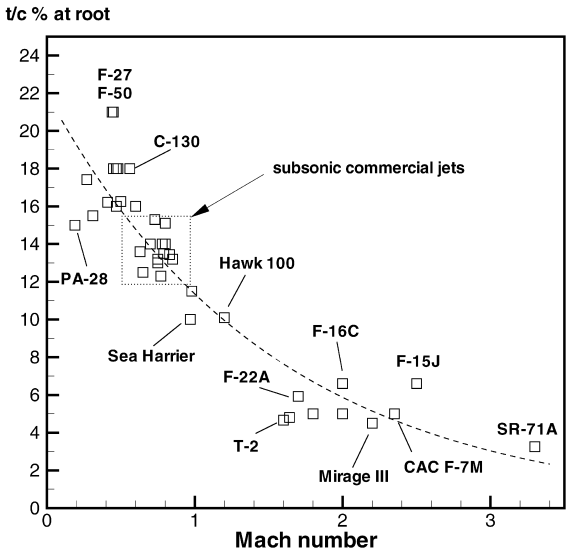

Fig. 13. Thickness ratio versus Mach number, all aircraft types.

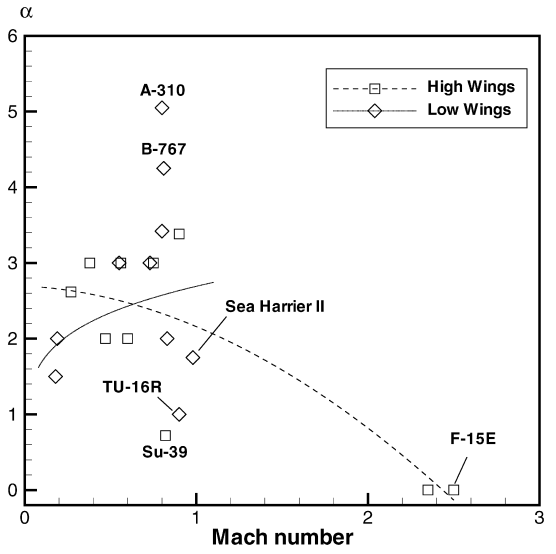

Fig. 14. Wing angle setting at root. Mach number is the long range cruise for civil aircraft, and maximum absolute speed for military vehicles. Dashed lines are power fit of the data.

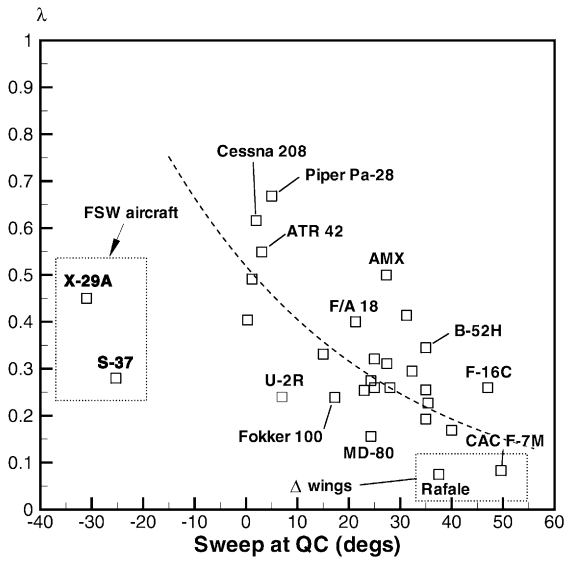

Fig. 15. Taper versus sweep versus sweep angle, all aircraft types.

5.6. Other geometrical characteristics

Dihedral and anhedral angles, β, are computed from the wing roots at the leading edge line. The accuracy is estimated at $\pm 30'$. The β values are very dependent on where the reference points are taken (quarter-chord, trailing-edge). Typical values are as follows: $\beta = -5$ to -2° for military cargos (high wing); $\beta = 5$–7° for commercial jet transports (low wing); $\beta = -10$ to 0 for supersonic jet fighters.

Boundary layer control is generally needed on the suction side of the wing. Typical devices include fences (F-102, BAe Hawk 200, Cessna 650) and vortex generators. The largest wings on record (Antonov An-124 and An-225) are clean.

The wing angle settings at the root, Fig. 14, are $\alpha_r \sim 1$–5 for business turboprops, zero (or nearly so) for most supersonic fighters. Most wings aircraft have a *washout*, e.g. a twist that is aimed at reducing the effective angle of attack at cruise conditions, and hence premature tip stall. Tip incidence can be negative.

The taper ratio $\lambda = c_t/c_r$ is shown in Fig. 15 in terms of the aircraft speed. The FSW aircraft have taper ratios of the same order as conventional supersonic wings.

The blade chord of most helicopters is constant, although the airfoil section may vary and the blade may be twisted (CH-47D, Mil-38). One notable exception is the tilt rotor Bell-Boeing V-22, which has a variable chord: $c_r = 0.90$ m, $c_t = 0.56$ m (this rotor has the characteristics of a large propeller).

Tip devices are now available on all the advanced vehicles. Typical features include winglets (most business jets, many commercial jets, some military aircraft), stabilizing floats (all amphibian vehicles), tanks (Aermacchi SF-260 and MB-339, Learjet 35A, Piper PA-42), Hoerner tips (some light aircraft, Fairchild A-10A). Rotorcraft tips are either swept back (AH-64D, Ka 52, Mil-28, Mil-38, S-90, Bell 222) or have a sophisticated contouring (ex. BERP tips on EH.101, NH.90, Westland Lynx).

6. Comparative analysis

We have performed some comparative analysis for the same class of aircraft, and across the whole spectrum of aircraft types. While some data show a relative scatter, others are remarkably clean. The data plotted refer only to the aircraft and rotorcraft in the database.

Each aircraft class has its own specific characteristics, from single-point design (most commercial vehicles), to multi-point design (virtually all the military vehicles).

6.1. Helicopters

The main rotor's technology comes in a number of different examples: single rotors (most vehicles), tandem/twin rotors (Boeing Vertol H-46, CH-47, Piasecki H-21), tilt rotors (Boeing-Sikorski V-22, Bell-Agusta BA-609), intermeshing rotors (Kaman K-max 1200), coaxial counter rotating (Kamov Ka-29, Ka-32, Ka-50, Ka-52, Ka-115, Ka-116, Ka-226A). The latter designs are tailless configurations. Tailless helicopters are also the

Table 4
rotorcraft data and performances (see nomenclature for symbols)[a]

Helicopter	Type	B	d	c	u	rpm	σ	μ	k	MTOW	W/A	h
Bell 209 SeaCobra	AT	2	13.41	0.84	333	311	0.0798	0.424	0.148	4535	32.11	
Bell 406/OH-58D	AT	4	10.67	0.24	232	395	0.0573	0.292	0.077	2500	27.96	2225
Bell 407	GE	4	10.67	0.27	237	413	0.0644	0.285	0.089	2270	25.39	3170
Bell 412	UT	4	14.02	0.40	230	314	0.0727	0.277	0.103	5260	34.07	1580
Bell AH-1W SuperCobra	AT	2	14.63	0.84	282	311	0.0731	0.329	0.175	6700	39.86	915
Bell 427	GE	4	11.28	0.27	250	395	0.0610	0.298	0.080	2835	28.37	4240
Bell/Boeing V-22	TR	3	11.61	0.76	185	333	0.1201	0.254	0.235	27,440	129.60	4330
BoeingVertol 114/CH-47D	TW	3	18.29	0.81	260	225	0.0846	0.335	0.132	24,500	46.62	1670
MD-500E	LC	5	8.05	0.17	248	492	0.0672	0.332	0.064	1360	26.74	1830
Enstrom 480	LC	3	9.75	0.24	204	334	0.0470	0.332	0.074	1300	17.32	3720
Aerospatiale 332	UT	4	15.60	0.60	266	265	0.0979	0.341	0.113	8600	44.99	2300
Aerospatiale 532	GE	4	15.60	0.60	262	265	0.0979	0.336	0.114	9000	47.09	1650
Aerospatiale 550	GE	3	10.69	0.35	248	394	0.0625	0.312	0.105	2250	25.07	2250
Aerospatiale 565N	GE	4	11.94	0.40	287	350	0.0853	0.364	0.092	4250	37.96	1200
Eurocopter EC 365N	GE	4	11.94	0.40	278	350	0.0853	0.353	0.095	4250	37.96	1200
Eurocopter BO 105	LC	4	9.84	0.27	240	424	0.0699	0.305	0.090	2500	32.87	455
Eurocopter EC 120B	LC	3	10.00	0.26	228	415	0.0497	0.291	0.089	1700	21.65	2530
Mitzubishi BK-117	GE	4	11.00	0.32	248	383	0.0741	0.312	0.093	3350	35.25	3000
Kaman Seasprite	UT	4	13.81	0.59	252	298	0.2176	0.325	0.132	6120	40.88	5845
Mil Mi-26	C	8	32.00	0.92	295	132	0.1464	0.371	0.078	56,000	69.63	1500
Mil Mi-28	AT	5	17.20	0.67	265	242	0.1240	0.338	0.115	11,400	49.06	3600

[a]Notes. (1) h is the hovering ceiling OGE. (2) V-22 has $c_r = 0.90\,\text{m}$, $c_t = 0.56\,\text{m}$; speed given in helicopter mode. (3) Bell 412: $c_r = 0.40\,\text{m}$, $c_t = 0.22\,\text{m}$. (4) Average blade chord for AS 565N, AS 365N, EC 155B: $c_r = 0.405\,\text{m}$, $c_t = 0.385\,\text{m}$. (5) Mil-26: largest helicopter; carries payload of same weight at Lockheed C-130J.

new series of light and utility vehicles MD 520 and MD 530. The number of blades ranges from 2 (most Bell helicopters) to 8 (Mil-26).

Rotor loadings give a measure of the aircraft size needed to lift a given gross weight, Stepniewski and Keys [38]. A partial list of data is presented in Table 4.

The rotor equivalent disk loading W/A is shown in Fig. 16, where the rotorcraft are compared at constant technology level. When exception is done for old technology (for example Sikorsky S-61 of the 1950s, Aerospatiale S321 of the 1960s, and a few others), the correlation is impressive.

The data of Fig. 16 have been separated into rotorcraft classes, and are well correlated by power fit curves, with a few exceptions: the G-vehicles of the Mil family (Mil-8, Mil-14, Mil-17, Mil-38) have unusually large diameters, hence a relatively low disk loading. However, they are aligned in their own design space. The T-vehicles are correlated by a linear fit, due to the low number of items on record. The bending of the fit curve is an indication of disk loading increasing at a faster pace than gross take-off weight. The tilt rotor Bell-Boeing V-22 has extraordinarily large disk loading, as does the heavy lift Sikorsky S-80/CH-53E (the performance of the V-22 is intended for helicopter mode).

Most of the data of A- , G- , U-vehicles fall within the power fit curves

$$W/A \sim 1.019\,W^{0.427}, \quad W/A \sim 0.202\,W^{0.592}, \tag{8}$$

where we assume the weight $W = \text{MTOW}$. The tail rotor diameter is also well correlated to the rotor disk loading by

$$\frac{D_{\text{tail}}}{D} \sim 0.127 \exp(8.2\,10^{-3} W/A). \tag{9}$$

Both data and correlation are shown in Fig. 17 (for helicopters having a tail rotor). EC 135 and EC 365N have a ducted tail rotor with staggered blades for reduced noise. Their design point is eccentric, but is has been considered in the determination of the curve fit.

The rotorcraft speed u is the maximum speed in forward flight at sea level. This is slightly lower than the absolute maximum speed (*never to exceed* speed), Fig. 8 (envelope 1). With this definition we can compare advance ratios and tip Mach numbers for different helicopters. The range of maximum speeds is 200–300 km/h. Only a few helicopters are capable of operating at higher speeds: MD AH-64D has $u_{\max} = 360\,\text{km/h}$; Lockheed

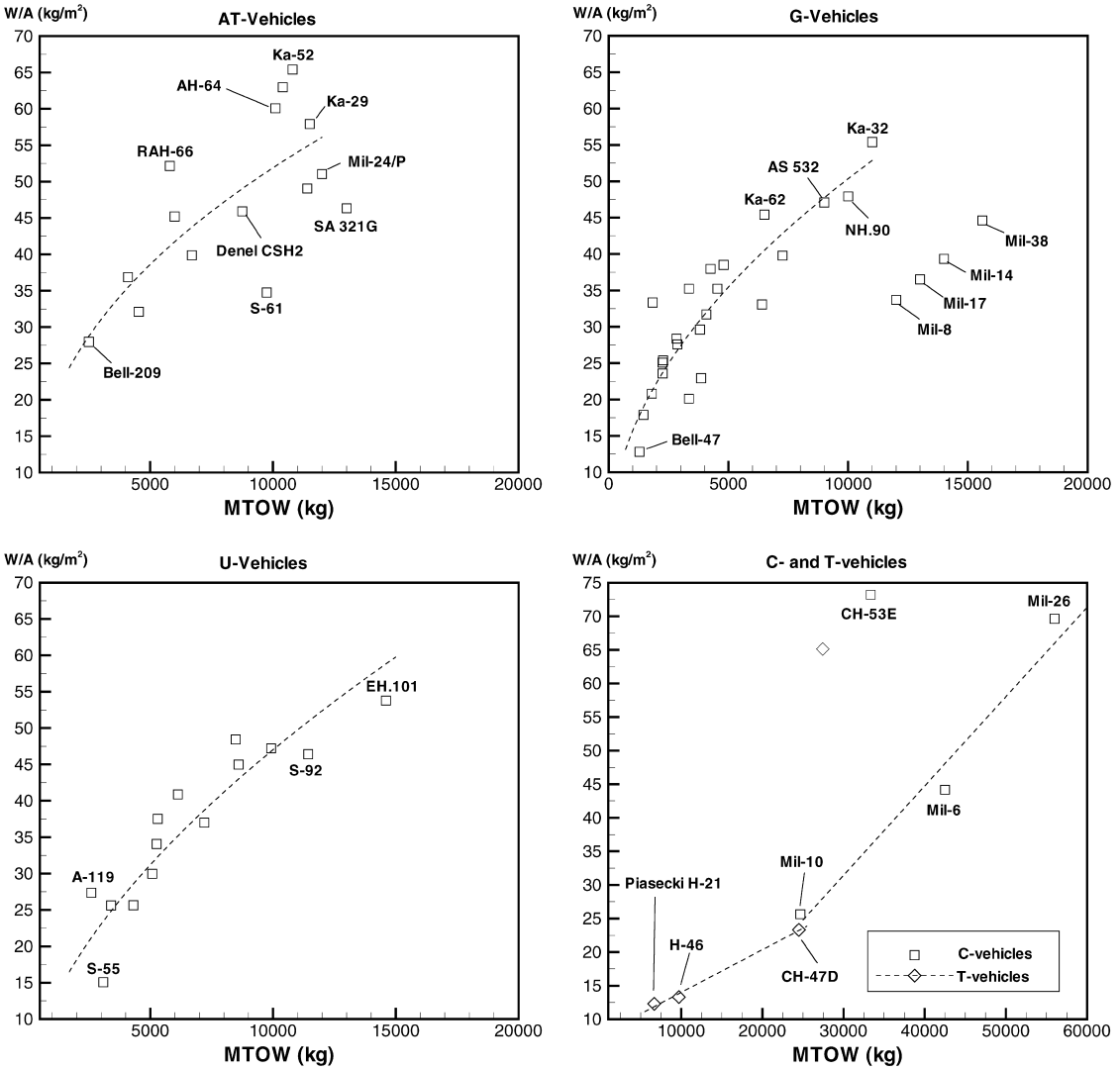

Fig. 16. Rotorcraft disk loading trends. Some vehicles are indicated to show extreme values of MTOW and W/A. Bell-47 was the first commercial helicopter (1947); Mil 26 is the largest vehicle in terms of MTOW. The G-vehicles are both civil and military general utility vehicles; the T-vehicles consist of tandem rotors, except the V-22 that is a tilt rotor.

AH-56 $u_{max} = 407$ km/h (though with compound thrust), due to limits imposed by flight instability, excessive tip Mach numbers, dynamic stall effects on rotating parts.

The main rotor's rpm reported in Table 4 are indicated as either constant or variable over a narrow range. Typical rotor speeds are 120–400 rpm. Some rotorcraft feature automatic control of the speed (for example, many helicopters of the Kamov series). Tail rotors turn at much higher rates, 1000–3000 rpm.

The computed tip Mach number is shown as a function of the maximum sea level speed (Fig. 18) and advance ratio (Fig. 19). The data are correlated by a line fit described by

$$M_{tip} = 1.031 \times 10^{-3} u + 0.603,$$

$$M_{tip} = 0.661\,\mu + 0.652, \tag{10}$$

where u is the sea level speed in km/h. An exception is the relatively low M_{tip} of the Enstrom 480, that features NACA 0012 airfoils sections. This airfoil is known for having poor transonic properties [39]: drag divergence is estimated at $M = 0.7$ at incidence $\alpha = 4^{\circ}$.

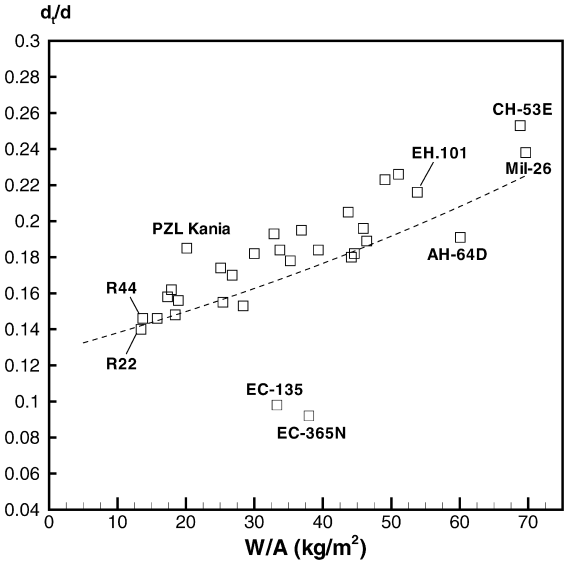

Fig. 17. Tail rotor relative size d_{tail}/d.

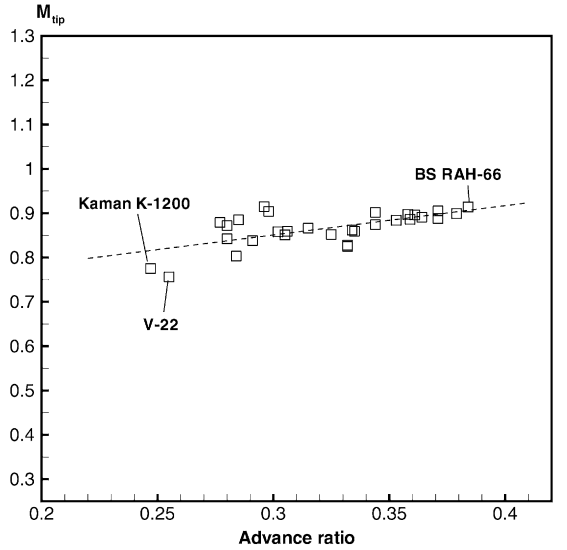

Fig. 19. Tip Mach number versus advance ratio μ.

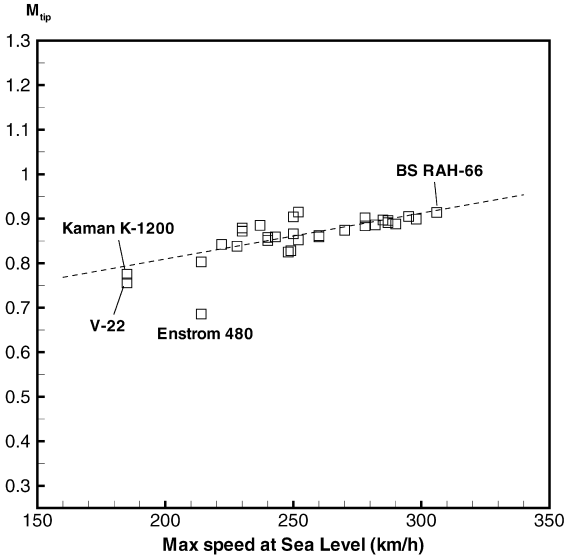

Fig. 18. Tip Mach number at maximum S/L speed. The performance for RAH-66 has been extrapolated from the maximum absolute speed.

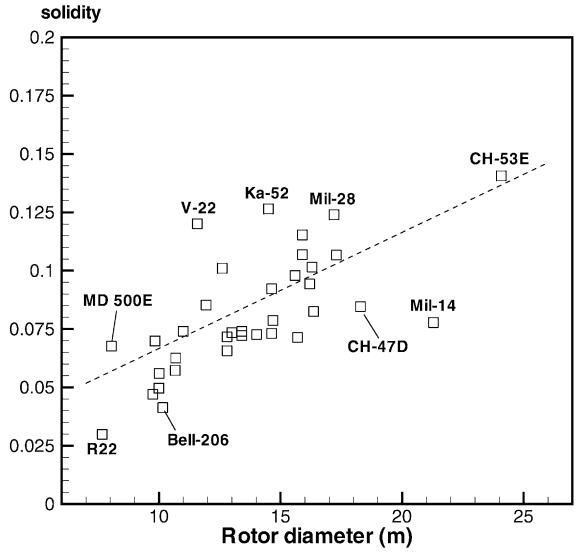

Fig. 20. Rotor solidity versus the diameter for all rotorcraft types. Value for V-22 is found from average blade chord $\bar{c} = 0.76$ m.

The rotor solidity, shown in Fig. 20 as a function of the rotor diameter, was computed from

$$\sigma = \frac{2\bar{c}B}{\pi D}. \tag{11}$$

A linear fit is a good approximation, although Mi-18 and V-22 are particularly eccentric: Mil Mi-18 is low because of the large diameter; V-22 is high because the blades are a compromise between helicopter rotor and aircraft propeller. The solidity of the Kamov Ka-52 has been computed by considering the rotor made of 6 blades (actual configuration is a 60° stagger between co-axial rotors). Most of the LC vehicles have solidity below the line fit.

The main rotor's reduced frequency at maximum sea level speed, defined by

$$k = \frac{\omega\bar{c}}{2u} \tag{12}$$

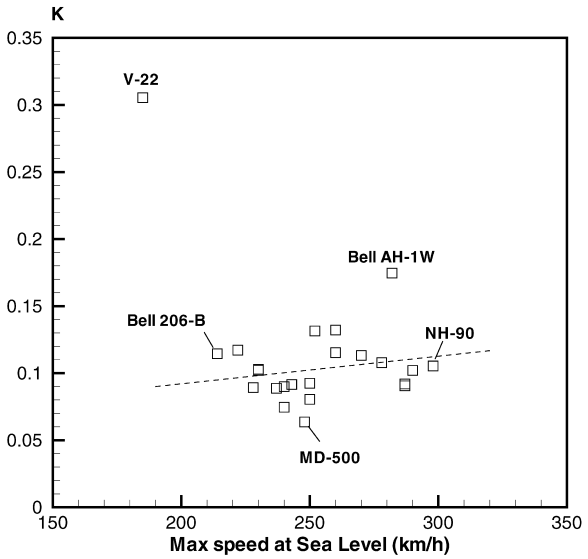

Fig. 21. Main rotor's reduced frequency at maximum sea level speed.

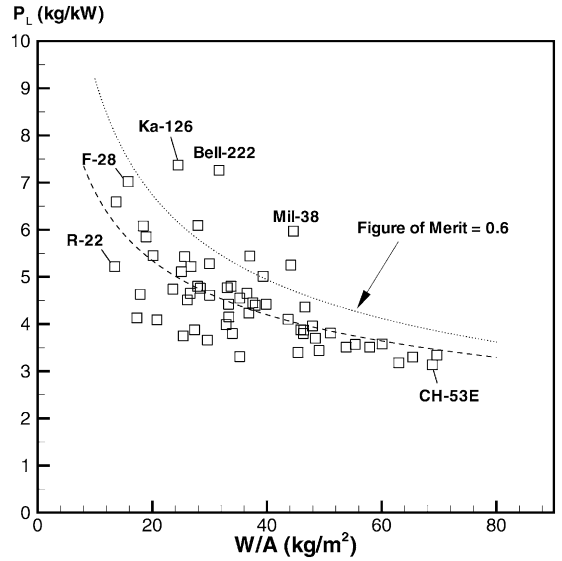

Fig. 22. Helicopter power loading. Line fit is a power curve through 62 operation points.

with $\omega = 2\pi$ rpm/60 is shown in Fig. 21. Most of the values are in the range 0.05–0.15. The line fit excludes the tilt-rotor V-22, which is particularly high. (This is however a limiting condition unlikely to be reached, since the vehicle is operated in the aircraft mode.) Relatively low forward speed is expected at high reduced frequencies, due to fatigue and aeroelastic limits imposed by the dynamic loadings on the rotor, even with advanced airfoil sections.

The main rotor performance is shown in Fig. 22 for all classes of vehicles. This is an indication of *deviation* from the ideal conditions of the power required for the static-thrust performance (hover). The rotor efficiency upper bound is about 0.6, with most of the rotors performing around 0.5.

6.2. Cargo aircraft

For no other aircraft type as the cargo the useful load fraction is so descriptive of the aircraft value. These aircraft are also the largest vehicles built, and their sheer size is undeniably fascinating. The data collected in Table 5 are a summary of characteristics of military vehicles and some vehicles re-engineered into military utility, from the small-size transport to the largest. All weights are expressed in metric tons (10^3 kg), and the figures of merit (described below) are for demonstrated performances of the aircraft versions specified in the table. Better performances are reported as records (for example, C-133) or design targets (An-225).

The Antonov An-225 is (on the design board) one and a half times heavier than a fully loaded Boeing B-747-400, while the Antonov An-124 is just 2% heavier. The An-225 at its design point, with its wing barely fitting on the long side of a football field (an amazing 88.40 metres), would be equivalent to 500 compact cars taking off at once.

Size effects on aircraft have been brilliantly discussed by Cleveland [9], who reversed an old opinion (for example, [40]) on the square/cube law. This law states that the structural stress increases with the characteristic length, as long as the load is proportional to the structural weight: in a W/A to MTOW map the correlation would be linear (this was also shown by Tennekes at all length scales [26]). Cleveland implied that this law would be defeated by technological advances, but this does not seem to be the case when comparing the aircraft of Table 5, even when larger aircraft than the Lockheed C-5 have been built. The data shown in Fig. 23 includes about 40 years of technology, and scaling seems appropriate, if we exclude the turboprops with substantially straight wing. Changes may be introduced in the future if more efficient engines become available, or if relatively old concepts such as the spanloader become a reality.

Considering the An-225 and G-222 (largest and smallest aircraft) the ratio between wing spans is 3, the ratio between wing areas is 9, and the ratios between gross weights is 18, which corresponds to a factor 2 in wing loading.

One figure of merit is the ratio between the payload and the empty operating weight, PAY/OWE, or the payload to gross take-off weight ratio, PAY/MTOW (*useful load fraction*). The graphics of Fig. 23 show the capability of each aircraft. Conventional wisdom would

Table 5
Data and performances of cargo and heavy lift aircraft (see nomenclature for symbols)[a]

Aircraft	$\mathscr{AR}$	b	Λ	β	M	P_L	R_C	MTOW	W/A	PAY	OWE	P/O	P/W
Alenia G-222/C-27	10.04	28.70	4.L	+ 2 30′	0.40	5.52	381	28.00	341	9.00	15.70	0.573	0.321
Antonov An-22 Antheus	12.00	64.40			0.50	5.59		250.00	725	80.00	114.00	0.702	0.320
Antonov An-70	9.0	44.06	17.L	− 5	0.65	3.16		130.00	602	47.00	72.80	0.646	0.362
Antonov An-124 Ruslan	8.55	73.30	28.Q	− 3 30′	0.80	440		405.00	645	150.00	175.00	0.857	0.370
Antonov An-225, Mryia	8.6	88.40	35.L	− 5 30′	0.76	435		508.20	663	156.30	na		0.308
Boeing KC-135A Stratolifter	7.04	39.88	34.L	+ 7	0.80	586	393	143.34	634	37.65	48.22	0.770	0.263
Boeing B-747-400F	7.67	64.44	37.Q	+ 7	0.82			396.90	730	113.00	181.50	0.623	0.285
Douglas C-133B Cargomaster	12.1	54.77			0.47	591	389	129.73	399		54.55		
Ilyushin Il-76MD	8.50	50.50	25.Q	− 3	0.77	361		190.00	567	47.00	89.00	0.528	0.247
Ilyushin Il-96T	8.48	57.66	30.Q	− 3	0.81	410		270.00	690	92.00	132.40	0.695	0.341
Lockheed C-141B StarLifter	7.92	48.74	29.L	− 3 30′	0.77	4.08	860	155.59	518	41.22	67.20	0.613	0.265
Lockheed C-130J Hercules	10.11	40.41	1.3L	+ 2 30′	0.56	5.70	640	70.30	434	21.80	34.30	0.636	0.310
Lockheed C-5B Galaxy	8.00	67.88	27.L	− 5 30′	0.78	496.	525	379.66	659	118.39	169.64	0.700	0.312
MD C-17A, Globemaster III	7.16	50.29	25.Q	− 4 30′	0.75	366		265.35	752	76.66	122.01	0.628	0.289
MD KC-10A, Extender	6.25	47.34	38.L	+ 4	0.76	382	884	267.62	739	76.84	110.95	0.693	0.287
SATIC A300-600, Beluga	7.7	44.84	28.Q	+ 6	0.70	295		155.00	425	47.30	86.40	0.547	0.305

[a]Note. (1) All swept back wings (sweep around LE or QC), except C-130J, C-133B, G-222, An-22. (2) Wing mounted high, except A300, KC-10A, KC-135A, Il-96T, B-747. (3) Winglets on Il-96T, C-17A. (4) Propulsion: C-141B, C-130J, An-22, An-70, G-222 are turboprops; others are jets. (5) Alenia G-222: sweep at outer panels. (6) Antonov An-22: largest propeller driven aircraft; 4-bladed counter-rotating propfans. (7) Antonov An-70: first aircraft to fly on propfans alone; propfans (8-bladed, 6-bladed counter-rotating); supercritical wing. (8) Antonov An-124: largest production aircraft; no fences, no vortex generators. (9) Antonov An-225: largest aircraft ever built; no fences, no vortex generators; design point: MTOW = 600,000 kg; PAY = 250,000 kg. (10) A300-600: aircraft with largest internal load capability; wing mounted low, with dihedral, based on A-300-600, with tip fences. (11) MD C-17 has NASA winglets; vectored thrust for improved STOL capability. (12) KC-10A: MTOW given for full cargo; tanker has lower MTOW, aircraft based on DC-10-30 wing. (13) KC-135: wing based on B717; MTOW given for full cargo; tanker version with lower MTOW.

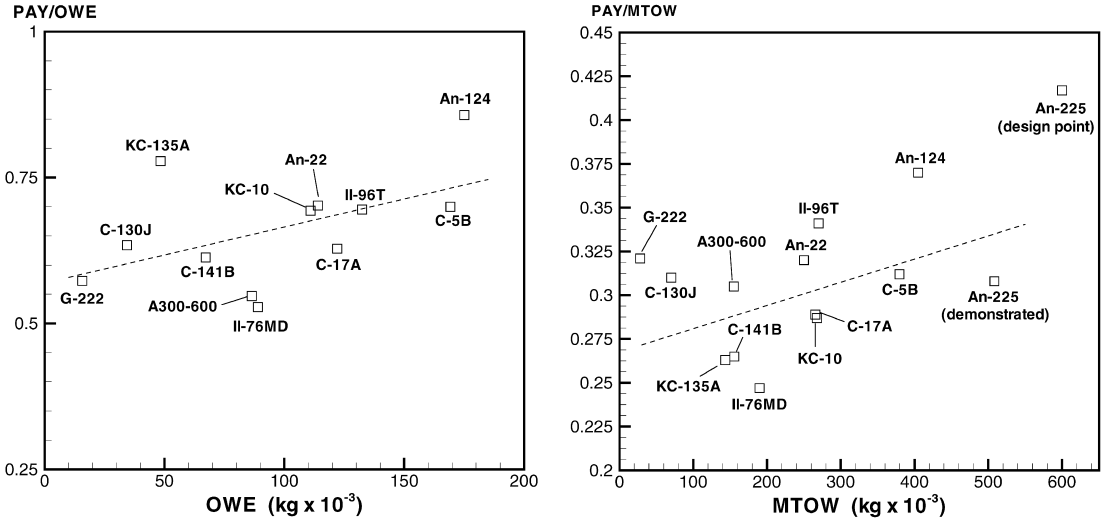

Fig. 23. Cargo aircraft PAY/OWE and and PAY/MTOW ratios versus aircraft size. (B747-4F = Boeing 747-400F).

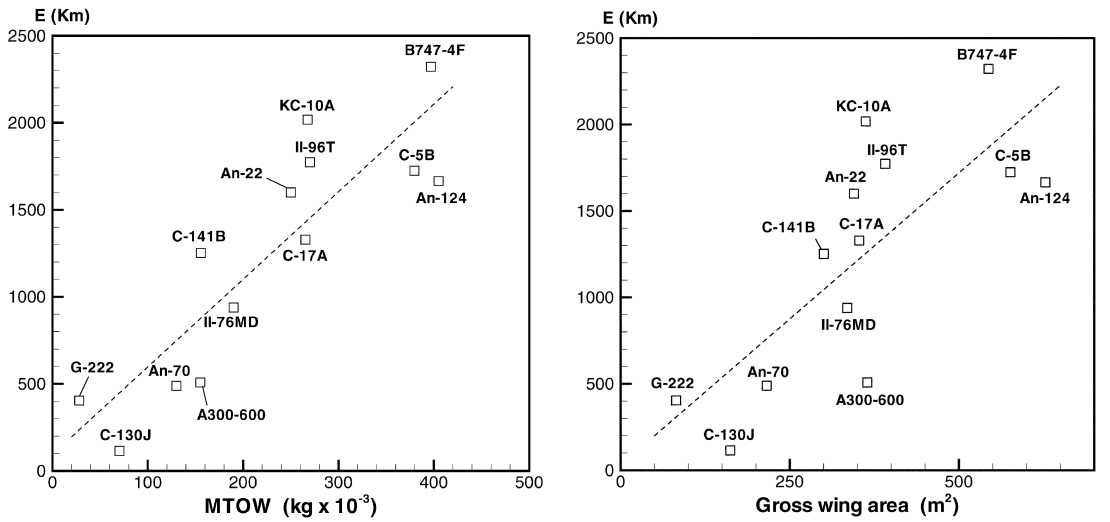

Fig. 24. Maximum cargo range.

suggest that it is more efficient to lift a few large cargos than several small ones, but relatively small airplanes, such as the Alenia G-222 and Lockheed C-130J have useful load fractions higher than many large airplanes. However, also the aircraft range must be used in the performance equation. The product PAY R (tons km) is biased toward the large aircraft; the product between the maximum useful load and the maximum aircraft range

$$E = \frac{\mathrm{PAY}}{\mathrm{MTOW}} R \tag{13}$$

is the *maximum cargo range*, and is given in km. This analysis is shown in Fig. 24. All the correlations are linear. There is a number of aircraft with gross wing area $A \sim 350\,\mathrm{m}^2$ (A300, C-17A, KC-10A, among others), showing that this aircraft size is the most commercially interesting. The large gap between A300-600 and KC-10A can be attributed to the fact that A300 is designed to carry internal oversize cargos (not necessarily bulky ones), while the KC-10A, working either as a cargo or tanker, can efficiently use all of its volume. The C-17 has operation point between A300 and KC-10A: its dimensions and payload have been designed to hold large units, like bulky military equipment.

The best figure is that of the Boeing B747-400F, which does not perform well in terms of absolute useful load, (Fig. 23). By comparison, the maximum cargo range of the Concorde is only 739 km, while the Airbus A340-300 has $E = 2700$ km.

6.3. Fighter jets

State-of-the-art fighters/attack aircraft are designed to operate at a wide range of speeds, weapons, external stores and missions. The data studied include aircraft primarily designed for air support (Harrier, A-10, JS37) and aircraft intended for air-to-ground operations (F-117).

Each point in the diagrams represents an optimum defining the best manoeuvring margins within costs limits of the aircraft operator. Variable wing sweep, transonic area rule design, low radar signature, advanced weapons systems are peculiar problems of this class of aircraft, that show the most scattered data and performances.

The flight envelope 4 of Fig. 8 is the limit performance. The aircraft can actually operate almost anywhere within this region. Useful references include reports of the AGARD Fluid Dynamics Panel [41] and [42], McMichael et al. [43], and Bradley [44].

Specific aerodynamic and system issues in fighter aircraft design include high-α performances, lateral and directional stability, aerodynamics of flight control, canard-wing interference, and radar cross-section. Some important performance parameters are the specific excess power and the maximum sustained rate of turn.

Specific excess power

$$P_s = \left(\frac{T-D}{W}\right)u = \frac{T}{W}u - \frac{\rho C_D u^3/2}{W/A}. \tag{14}$$

For a given altitude and speed (single point in the flight envelope diagram, Fig. 8), P_s can be maximized by high thrust rating, high wing loading (hence small wings) and low C_D. At given C_D and flight altitude P_s is a function of both T/W and W/A, that are considered the most important parameters affecting the aircraft performance. Fig. 25 shows the T/W and W/A data obtained at sea level. For reference, also 3 lines of constant P_s have been computed, using a ground speed $M = 0.9$ and a drag coefficient $C_D = 0.4$. At altitude, the T/W and W/A are only a fraction of the data presented, and changes are dependent on the particular aircraft, on the number of external stores left for close-in-combat flight, and engine efficiency.

It is easy to see using average data in Eq. (14) that P_s becomes a large negative number, which means the drag rise is in excess of the available thrust. Although the data at sea level cannot actually be scaled at altitude, Fig. 25 gives an indication of system effectiveness, in particular an indication of power available for sustained turn rates. The fighter Lockheed F-22A claims $T/W = 1.117$ at take-off, while the maximum value is indicated as $T/W = 1.42$.

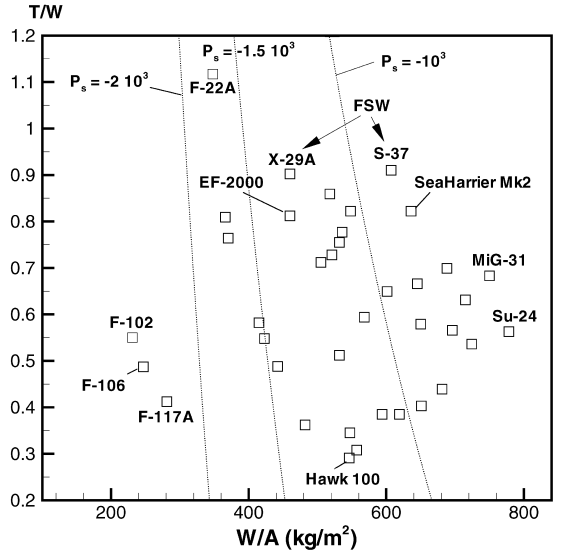

Fig. 25. Thrust-to-weight data for supersonic jet fighters. Data elaborated from maximum thrust rating with afterburning and MTOW at sea level.

There is a considerable scatter in the data. Tornado ADV is off scale with a theoretical wing loading of about 1000 kg/m^2. At the other end there are aircraft with $W/A \sim 350$–800 kg/m^2.

The *maximum sustained rate of turn* is

$$\dot{\Theta} = \frac{g}{u}(n^2-1)^{1/2}\frac{\pi}{180}\,(\text{rad/s}), \tag{15}$$

where n is the normal load factor. The turn is generally performed in highly unsteady flight. Therefore, a third performance parameter is defined: the *maximum instantaneous load factor*

$$n_z = \frac{C_{L_{max}} q}{W/A}, \tag{16}$$

which is limited by the structural resistance of the aircraft. Evaluation of the $C_{L_{max}}$ is neither straightforward, nor easily available in the technical literature.

The number of parameters needed to fully characterize a fighter/attack aircraft is in the order of several dozens. The data available are rather sparse, because of sensitive importance. However, they include the following: roll rates of up to 270°/s; AoA up to 50 or 80° (FSW aircraft); max sustained turn rates of the order of 10°/s; max instantaneous load factor up to 9g; max specific excess power 150 m/s; max acceleration through the sound barrier 0.5g in straight flight; max rate of climb over

Table 6
Selected data and performances of fighters (see nomenclature for symbols)[a]

Aircraft	Wing	Λ	b	$\mathscr{AR}$	β	M	MTOW	g^+	R_C	Z	U_s	A	W/A	T/W
AMX	SB	31 LE	8.87	3.75	−2	0.86	13,000	7.3	3124	13,000		21.0	619	0.385
BAe SeaHarrier Mk2	SB	34 QC	7.70	3.55	−12	0.97	11,890	7.8			177	16.7	636	0.822
Boeing F/A 18E	SB	37 LE	13.62	4.00	−2 30′	1.80	29,950	7.5		15,250		46.5	645	0.666
Ching-Kuo (Taiwan)	SB-V	28 LE	8.53	3.00	0	1.80	12,750	6.5	15,240	16,670	186	24.3	505	0.712
Dassault Mirage 2K	Δ	58 LE	9.13	2.03		2.20	17,000	9.0	18,300	17,000	180	41.0	415	0.582
Eurofighter 2000	Δ	53 LE	10.95	2.40		2.00	23,000	9.0				50.0	460	0.812
Fairchild A-10	UW		17.53	6.54		0.78	22,680		1830			47.0	482	0.362
General Dyn F111/F	VSW	72 LE	9.74		0	2.50	45,360			18,000		61.0		0.502
Grumman F-14A	VSW	69 LE	11.65			2.34	33,270		9140	15,240	213	52.5		0.570
Lockheed F-22A	Δ	49 LE	13.56	2.36	−3	1.70	27,200	9.0		15,250		78.0	348	1.117
Lockheed F-16C	Δ	39 LE	9.45	3.20		2.00	19,200	9.0		15,250			688	0.699
Lockheed F-117A	BWB	67 LE	13.20			0.97	23,800	6.0		16,765		84.8	281	0.412
MAPO MiG-29	SB	42 LE	11.36	3.40	−2	2.30	19,700	9.0	19,800	18,000		38.0	518	0.859
MAPO MiG-31	SB	41 LE	13.47	2.95	−4	2.83	46,200	9.0		20,600		61.6	750	0.683
NAMC Q-5 (China)	SB	57 LE	9.68	3.35	−4	1.20	11,830	7.5	8880	15,850		28.0	423	0.548
SAAB Viggen JA37	Δ^2		10.60	2.40		2.00	17,000						370	0.764
SAAB Gripen JS39	Δ	45 LE	8.40			2.00	13,000	9.0						0.644
Sukhoi Su-27	SB	42 LE	14.70	3.49	0	2.35	33,000	9.0		18,000	200	62.0	532	0.755
Sukhoi Su-34	SB	42 LE	14.70	3.49		1.80	44,350			19,800		62.0	715	0.631
Tornado ADV	VSW	67 LE	8.60		−5	2.20	28,000	7.5		21,330			na	0.698

[a]Note. (1) VSW-aircraft: wing span, areas and $\mathscr{AR}$ given at maximum sweep angle. (2) Dihedral/anhedral angles estimated from roots, with aircraft on the ground. (3) R_C at sea level for: AMX, Hawk 100 NAMC Q-5, A-10. (4) Dog-tooth LE line on Lockheed F/A 18E, SAAB JS 39. (5) Thrust vectoring on: F-22A (max deflection 22 degs down); Su-27; BAe Sea Harrier. (6) F-117A is not technically a fighter, because not designed for air-to-air combat. (7) MD F-111: sweep continuously variable from 16 to 72°. (8) Eurofighter 2000: tailess delta wing, mounted low. (9) JS39 Gripen: Mach number unconfirmed. (10) JA37 Viggen: canards with TE flaps for aircraft control at high AoA. (11) Dassault Rafale: movable canards, up to 20°.

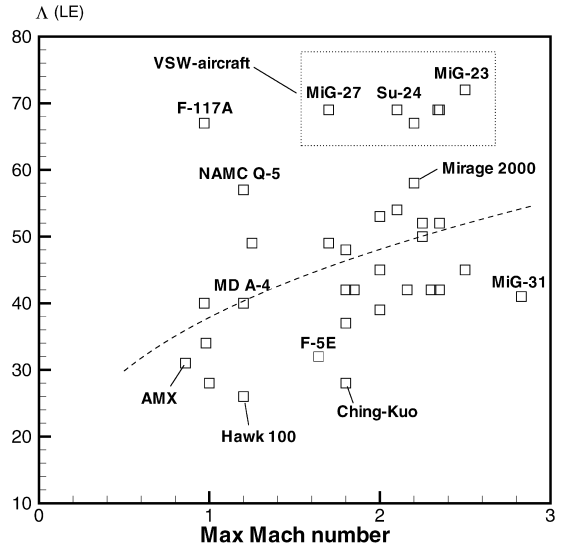

Fig. 26. Fighter aircraft Mach number plotted versus the wing sweep at LE. For the VSW aircraft sweep has been considered at fully spread wings.

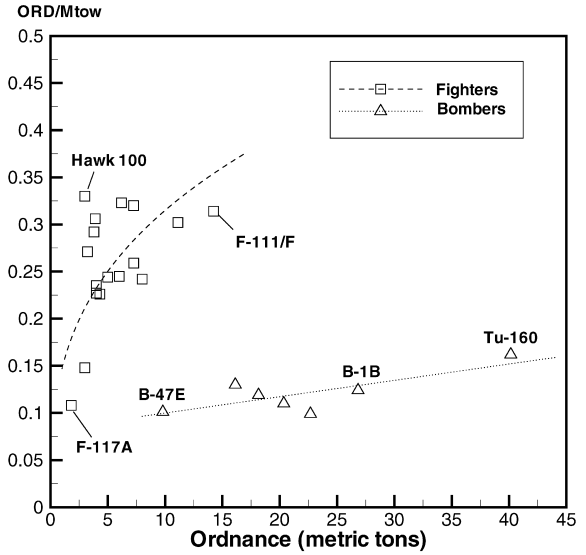

Fig. 27. Ordnance-to-MTOW ratios for bombers and fighters.

19,000 m/min; max weapons load ratios of 0.25; supercruise at sea level $M = 1.2$; take-off runs assisted by afterburning as low as 0.25 km (half of this on ramp).

Most of the data on record show a large scatter, which is a sign that design, mission requirements and performances change considerably from one aircraft to the other. A quick look at the basic parameters of the wing system (see Table 6 for reference) would suggest so. Scaling is not an issue, like for the cargo aircraft discussed above: aerodynamic characteristics, stability margins, control surface sizing, power plants, landing gear, and flight controls do not scale with aircraft size.

Wind tunnel test times, as shown in Fig. 1, have been growing to over 20,000 h (all aerodynamic sub-components, full configuration system, and all speed ranges), although the experimental research aircraft Grumman X-29A required less than 1200 h before maiden flight in 1984 [45]. This was in the same order as the development of the F-101 30 years earlier.

Fig. 26 shows the fighters Mach number in supersonic dash as function of the wing aspect-ratio. The VSW-aircraft are plotted at the operation point corresponding to maximum sweep Λ_{LE}, and are placed above the power fit line. The Λ of F-117A is far larger than the one required to fly at the corresponding speed. This is due to its design for low radar signature. The wing of NAMC Q-5 is unusually swept, while the top speed claimed is barely above $M = 1$. The MiG-31 claims a top speed $M = 2.83$. Mach = 2.5 is the practical speed limit for aero-thermodynamic heat stress of today's aircraft (this corresponds to a stagnation temperature of about 250°C). Even at $M = 2.5$ this aircraft covers about 32 body lengths/second (while the F-15E covers 38 body lengths at the same speed).

Some ratios between maximum war-load weight and MTOW have been extrapolated, although it is difficult to work out the details (internal and external bays, optional loads, barrel guns, etc.). For fighter aircraft this ratio is in the range 0.10–0.30; for heavy bombers estimates give 0.10–0.14 (largest for Tupolev Tu-160). The maximum ordnance to gross weight for both bombers and fighters/attack aircraft is shown in Fig. 27. The Lockheed F-117A is not technically a fighter, although it has been classified so; its maximum weapons load seems aligned with that of the bombers.

6.4. Subsonic commercial jets

Flying faster and more efficiently has been the main goal since the beginning of commercial and passenger transport. Fig. 28 shows the speed of commercial airplanes at year of first flight. The speed of piston engines continued to grow until the late 1940s. The introduction of the jet engines appeared before the speed reached the intrinsic limit of propeller-driven aircraft, and the cruise speed kept increasing. The introduction of new supercritical wing sections has allowed a further gain of $M \sim 0.05$, but then a transonic limit of about 0.82 was reached in the early 1970s. It has remained as such for the past 30 years. Further increases are not expected. Innovations such as transonic area ruling design (a relatively old concept) could increase the drag divergence point by $M \sim 0.1$, but it is considered not feasible because of the increased airframe costs.

The Boeing B-707 featured a very advanced technology, having been introduced at about the same time as

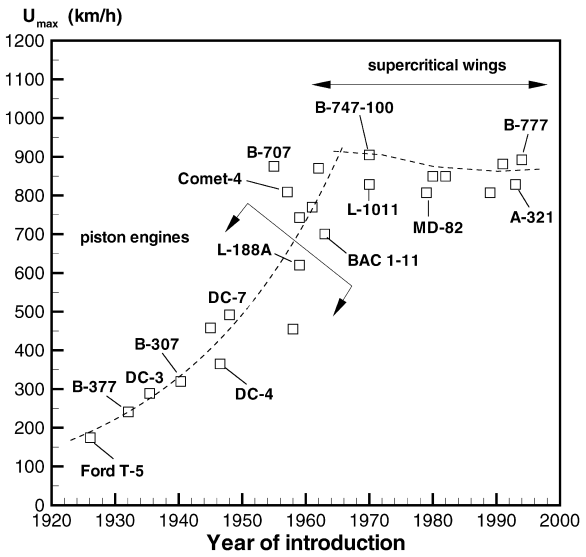

Fig. 28. Demonstrated cruise speeds of airliners at year of introduction.

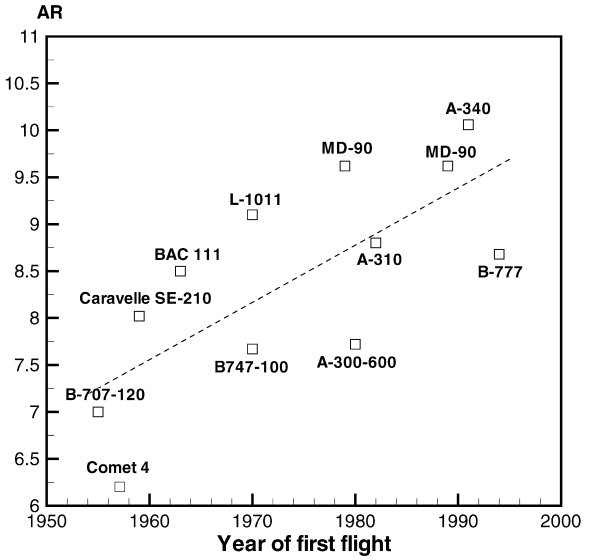

Fig. 30. Wing aspect-ratio of airliners at year of introduction.

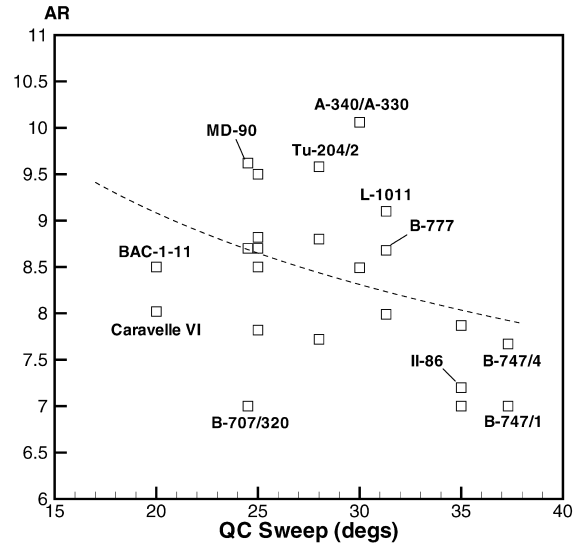

Fig. 29. Wing sweep versus $\mathscr{A}\mathscr{R}$ for commercial subsonic transport aircraft.

the Lockheed L-049 Constellation and a few other propeller aircraft. The jet revolution has consolidated a philosophy in aircraft design that it is difficult to challenge: cylindrical fuselage, swept back wings (Fig. 29), multislotted control surfaces (Fig. 7).

Improvement of aerodynamic efficiency is one of the key aerodynamic problems in this class of aircraft. Aerodynamic interference, skin friction and induced drag are the most promising areas of research.

For given span efficiency, the induced drag is an inverse function of the aspect-ratio, as described by Eq. (1). The tendency has been toward decreasing the wing sweep and increasing the wing span (Fig. 30). This progress has been facilitated by the introduction of supercritical wing sections and winglets (MD-11, B-747-400, B-777, A310-300, A340-300, Il-96, Tu-204D). Some aspect-ratios now are around 10 (MD-90, Airbus A-340), while many others are slightly below 9. In the early days of jet propulsion commercial aircraft had wing aspect-ratios of the order 6–7. Poisson-Quinton [25] predicted a L/D for subsonic long range cruise conditions growing with the wing span according to

$$\frac{L}{D} = 14\frac{b}{\sqrt{A_{\text{wet}}}}, \tag{17}$$

assuming a span efficiency $e = 0.75$ and a skin friction coefficient $c_f = 0.003$. The useful load fraction ratio PAY/MTOW is in the range 0.21–0.31. In comparison, the only supersonic transport flying at present, the Concorde, has PAY/OWE ~ 0.11.

7. Perspectives and conclusions

In this article we have presented a summary of aircraft and rotorcraft characteristics taken from full-scale data and from flight performances. The vehicles selected were mostly from the last 40 years of aircraft design.

The analysis shows that in many cases interesting correlations can be obtained. Also, highlighted historical trends, the effects of regulations on noise emissions, and

the state-of-the-art values for several classes of aircraft and rotorcraft. The use of this database is expected to be useful for aircraft design, propulsion systems analysis, and aerodynamic benchmark. Where is aeronautics heading?

Igor Sikorsky wrote in 1958 that "Supersonic aeroplanes have carried men at more than 2000 miles per hour and there are reasons to believe that this speed will be doubled by 1960 or so…" [46].

In 1970 Cleveland wrote that "future growth potential looks unlimited… one gross weight doubling, and possibly two, is predicted by 1985; nuclear power can drive [the aircraft's] optimum weight to 5 or 10 million pounds before the year 2000" [9].

These and other predictions turned out to be wrong. In truth, the increasing level of technology has also increased the resilience of the industry to pursue changes, so that many alternative ideas (for example, the oblique wing [47], the twin fuselage [48], the joined wing [49], the blended wing body [50]) have not been exploited.

Note to readers. The full database discussed in this article [1] is available on request to non-profit institutions committed to the advancement of aerospace sciences.

References

[1] Filippone A. Aerospace data base: aircraft and rotorcraft. Technical Report DTU-ET-AFM-2000-01, April 2000.

[2] Lange RH. Trends in very large aircraft design and technology. AIAA Paper 80-0902, 1980.

[3] Jackson P, editor. Jane's all the world's aircraft. Jane's Information Systems (published every year).

[4] Anonymous. A simpler way to build complex aircraft. Aerospace America, September 1999, p. 22.

[5] Seckel E. Stability and control of aircraft and helicopters. Reading, MA: Addison-Wesley, 1964.

[6] Handler EH. Tilt and vertical float aircraft for open ocean operations. J Aircraft 1970;3(6):481–9.

[7] Nelms WP, Anderson SB. V/STOL concepts in the United States: past, present and future. Special Course on V/STOL Aerodynamics, AGARD R-710, 1984.

[8] Gurton B. The encyclopedia of Russian aircraft 1875–1995. Osceola, WI 54020, USA: Motorbooks International Publishers & Wholesalers, 1995.

[9] Cleveland FA. Size effects in conventional aircraft design. J Aircraft 1970;7(6):483–512.

[10] Poisson-Quinton Ph. Energy conservation aircraft design and operational procedures. Aircraft Engine Future Fuels and Energy Conservation, AGARD LS-96, 1984.

[11] Loftkin LK. Aeronautical vehicles — 1970 and beyond. J Aircraft 1971;8(12):939–51.

[12] Küchemann D. The aerodynamic design of aircraft. Oxford: Pergamon Press, 1978.

[13] Stinton D. The anatomy of the aeroplane. London: G.T. Foulis and Co. Ltd., 1966.

[14] AIAA. Aerospace design engineers guide, 4th ed. 1998.

[15] Hopps RH, Danforth ECB. Correlation of wind tunnel and flight test data for the Lockheed L-1011 Tristar airplane. Performance prediction methods, AGARD CP-242, 1977.

[16] Haftmann B, Debbeler FJ, Gielen H. Take-off drag prediction for Airbus A300-600 and A310 compared with flight test results. J. Aircraft 1988;25(12):1088–96.

[17] Obert E. Forty years of high-lift R & D — An aircraft manifacturer's experience. AGARD CP-515, High-Lift Systems Aerodynamics, September 1993.

[18] Olason ML, Norton DA. Aerodynamic design philosophy of the Boeing 737. J Aircraft 1966;3(6):524–8.

[19] Shevell RS, Schaufele RD. Aerodynamic design features of the DC-9. J Aircraft 1966;3(6):515–23.

[20] Chandrasekaren RM. Computational aerodynamic design of the Gulfstream IV. AIAA Paper 85-0427, 1985.

[21] Hefner, Bushnell DM. An overview of concepts for aircraft drag reduction. Special Course on Concepts for Aircraft Drag Reduction, AGARD R-654. 1977.

[22] Bore CL. Airframe/store integration. Special Course on Fundamentals of Fighter Aircraft Design, AGARD R-740. 1987.

[23] Robert JP. Drag reduction: an industrial challenge. Special Course on Skin Friction Drag Reduction, AGARD R-786, March 1992.

[24] Gallagher JG. Aerodynamic prediction methods at low speeds with mechanical high-lift devices. Prediction Methods for Aircraft Aerodynamic Characteristics, AGARD LS-67, 1974.

[25] Poisson-Quinton Ph. Parassitic and interference drag prediction and reduction. Aircraft Drag Prediction and Reduction, AGARD R-723, 1985.

[26] Tennekes H. The simple science of flight. Cambridge: The MIT Press, 1993.

[27] Kroo I, McMasters J, Smith SC. Highly nonplanar lifting systems. Transportation Beyond 2000, NASA CP 10184, NASA Langley Research Center, 1996.

[28] Ashley H. Engineering analysis of flight vehicles. Reading, MA: Addison-Wesley, 1974.

[29] Ashley H, Landahl M. Aerodynamics of wings and bodies. Reading, MA: Addison-Wesley, 1965.

[30] Goodmanson LT, Gratzer LB. Recent advances in aerodynamics for transport aircraft. Prog Aeronaut Astronaut 1973;11(12):30–45.

[31] Cochrane RJ, Carras JA. Hybrid upper surface blown flap propulsive lift concept for the QSRA. J Aircraft 1976;13(11):855–60.

[32] High-Lift Systems Aerodynamics, AGARD CP-515, September 1993.

[33] Crighton DG. Model equations of nonlinear acoustics. Annu Rev Fluid Mech 1979;11:11–33.

[34] Lowson MV. New prediction methods for helicopter noise. 19th European Rotorcraft Forum, vol. I, Como, Italy, September 1993. Paper B7.

[35] Cox C. Helicopter noise certification experience and compliance cost reductions. 19th European Rotorcraft Forum, Como, Italy, September 1993. Paper E1.

[36] Raymer D. Aircraft design: a conceptual approach. AIAA educational series, 3rd ed. 1998 [Chapter 3].

[37] Conner DA, Wellman JB. Hover acoustic characteristics of the XV-15 with advanced technology blades. J Aircraft 1994;31(4):737–44.
[38] Stepniewski WZ, Keys CN. Rotary-wing aerodynamics. New York: Dover Publ., 1984.
[39] Abbott IH, Von Doenhoff AE. Theory of wing sections. New York: Dover Publ., Inc., 1959.
[40] Durand WF. Some outstanding problems in aeronautics. J Roy Aeronaut Soc 1953;57(516). p. 805.
[41] Special Course on Fundamentals of Fighter Aircraft Design, AGARD R-740, October 1987.
[42] Loads and Requirements for Military Technology, AGARD AR-815, February 1997.
[43] McMichael T, McKay K, Walker MJ, Fielding C, Lockley G, Curtis P, Probert B, Lee CS, Moretti G. Aerodynamic technology — The role of aerodynamic technology in the design and development of modern combat aircraft. Aeronaut J 1996;100(1000):411–24.
[44] Bradley RG. Practical aerodynamic problems — military aircraft. Progress in aeronautics and astronautics, vol. 81, Transonic aerodynamics. AIAA, 1982.
[45] Boppe J. Aerodynamic drag analysis methods. Engineering Methods in Aerodynamic Analysis and Design of Aircraft, AGARD R-783, 1992.
[46] Lambermont P, Pirie A. Helicopters and autogyros of the world. London: Cassell, 1958.
[47] Jones RT, Nisbet JW. Transonic transport wings — oblique or swept? Aeronaut Astronaut 1974;40–7.
[48] Houbolt JC. Why twin-fuselage aircraft? Astronautics and Aeronautics 1982;26–35.
[49] Wolkovitch J. The joined wing: an overview. J Aircraft 1986;23(1):161–78.
[50] Liebeck RH, Page MA, Rawdon BK, Scott PW, Wright RA. Concepts for advanced subsonic transports. NASA CR-4624. 1994.